GEOLOGY FOR SOCIETY

SINCE 1858

GEOLOGICAL
SURVEY OF
NORWAY

· NGU ·

NORGES GEOLOGISKE UNDERSØKELSE
- NGU -

REPORT

Geological Survey of Norway
P.O. Box 6315 Torgarden
NO-7491 TRONDHEIM

Report no.: 2019.009	**ISSN: 0800-3416 (print)** **ISSN: 2387-3515 (online)**	**Grading**: Open

Title: Magnetotelluric 2D inversion and joint interpretation of MT, seismic, magnetic and gravity data from Masi, Kautokeino municipality, Finnmark

Authors: Frida Mathayo Mrope, Michael Becken, Bent Ole Ruud, Odleiv Olesen, Tor Arne Johansen, Marco Brönner, Sofie Gradmann and Aziz Nasuti	**Client:** NGU
County: Finnmark	**municipality**: Kautokeino
Map-sheet name (M=1:250.000) Nordreisa	**Map-sheet no. and -name (M=1:50.000)** 1933 IV MASI
Deposit name and grid-reference:	**Number of pages**: 64 Price (NOK): 225

Fieldwork carried out: 2015	**Date of report**: 1st March, 2019	**Project no.**: 347100	**Person responsible**:

Summary: Acquisition of Magnetotelluric (MT) data at Masi is a joint venture project between NGU and Westfälische Wilhelms Universitat Münster in Germany. The data was collected in 2015. The main objective is to understand the regional geology in the area and especially the settings of the postglacial Stuoragurra Fault. The project area has been extensively studied and a considerable amount of information about the geology is available. However, most of this information provides only knowledge of the shallow subsurface. Having a range of high to low frequencies, MT data has a great depth of penetration and is hence a useful tool in understanding the deep subsurface.

Interpretation of the resistivity model was done by integrating the geological bedrock map, seismic section, 2D resistivity profiles, resistivity log and magnetic and gravity data. The deep structures observed in the MT model guided the interpretation of the gravity and magnetic data and hence minimized the number of possible models.

The final resistivity model shows four distinct zones. Zone 1 is characterized by low resistivity in the west. It is interpreted as an interbedding of amphibolites, mica schists and black schists overlaying the Masi quartzite. Zone 2 is a relatively high-resistive unit alternating with low-resistivity sections to the east. It is interpreted as fractured Masi quartzite intruded by albite diabase. To the east of the Masi quartzite are the Gål'denvarri amphibolite and a granodiorite. Zone 3 is a high-resistive layer spanning the entire profile below zones 1 and 2. It is interpreted as granite and/or gneiss. Zone 4 is a relatively low-resistive layer underlying zone 3. It is interpreted as an intermediate gneiss.

The Stuoragurra Fault (SF) is located within the Mierujavri-Sværholt Fault Zone (MSFZ) and represent a fractured section of zone 2. The SF is interpreted to be about 2 km wide whereas the MSFZ is about 6 km wide. A dense receiver spacing (500 m) and higher frequencies of up to 90 Hz enhanced the MT resolution for imaging the structures in the shallow subsurface.

Keywords: Magnetotellurics	MARE2DEM 2D inversion	Resistivity
Seismic	Airborne magnetic data	Gravity data
Scientific report	Geophysics	

CONTENT

FIGURES

TABLES

1. INTRODUCTION

1.1. The project objective

This report covers 2D inversion and interpretation work of magnetotelluric (MT) data from Masi. The MT data was collected in the summer of 2015 and was processed at the University of Münster, Germany. In 2018 the data was inverted at NGU and the results are presented here. The interpretation is based on the electrical resistivity distribution in the subsurface and its correlation with the available geological and geophysical information: bedrock map, seismic sections, 2D resistivity profiles, resistivity logs, magnetic and gravity data.

The main objective is to understand the regional geology in the area and especially the settings of the postglacial Stuoragurra Fault which strikes NNE-SSW. The project area has been extensively studied and a considerable amount of information about the geology is available. However, most of this information provides only knowledge of the shallow subsurface. With a range of high to low frequencies, MT data has a great depth of penetration and is therefore a useful tool in the understanding of the deep subsurface.

Masi is located in the Kautokeino municipality, Finnmark county, northern Norway (Figure 1). The project area is in the north of the Masi village and it lies between 593990 and 612035 Eastings and 7706525 and 7711720 Northings (UTM zone 34). The MT profile is indicated in Figure 1 by the red line.
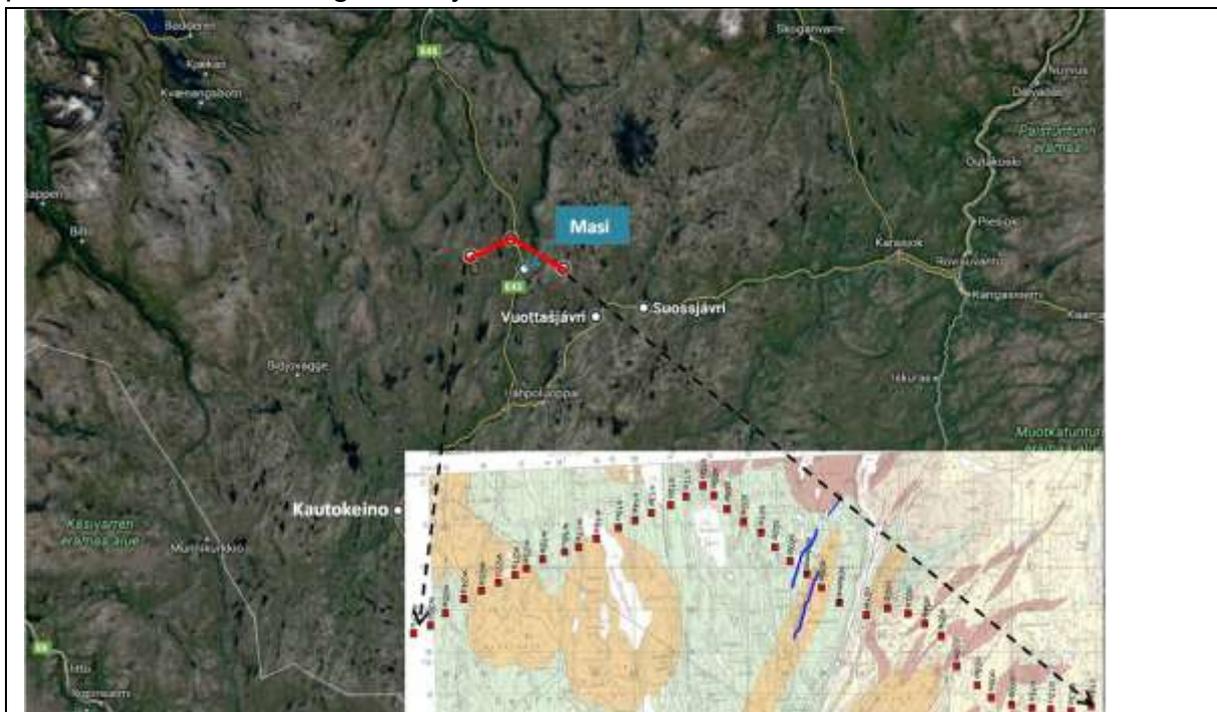
Figure 1: An overview of the survey area in the Kautokeino municipality. The location of the MT profile is shown by the red line near the Masi village. The image at the bottom right shows the survey layout and the location of the Stuoragurra Fault is indicated by the blue lines.

1.2. The report outline

Apart from the general information on the geological settings, the MT method and the inversion code, this report presents:

- 2D inversion of synthetic data. Since this is the first MT inversion project at NGU using a MARE2DEM code, a test was performed on synthetic data to build confidence on the results of the real data. In addition, tests on the synthetic data provide a rough idea on inversion parameters suitable for the subject area.
- Preliminary results of the Masi MT data inversion. The inversion was run using default inversion parameters for initial evaluation of the input data. The problematic data points normally show up with extreme misfits.
- Starting models and inversion parameter tests. The results of the different tests are shown in the appendix. The tests aim at finding the best parameters for optimal results.
- Results of the final 2D inversion. The model is examined qualitatively and quantitatively by visual inspection and by a misfit analysis, respectively. The observations are described.
- Reflection seismic acquisition and processing. The Masi MT data was acquired along a profile where seismic data was earlier acquired. The seismic profile will be jointly analysed with the MT result and hence its acquisition and processing steps are briefly explained.
- Interpretation of the final resistivity model. The result of the MT inversion gives the resistivity distribution of the subsurface. By integration with other available information, the resistivity model is geologically interpreted. The bedrock map shows different lithologies mapped on the surface. The resistivity of these lithologies has been measured using DC resistivity profiles and well logs.
    - The first step in the interpretation of the MT profile is a comparison of the resistivities of the known lithologies as observed in the well log, DC resistivity profiles and that of the MT profile. The agreement of the resistivity ranges in the different resistivity methods gives confidence to the MT inverse model.
    - The second step is joint interpretation of the MT, seismic, magnetic and gravity data. The MT resistivity model (image) superimposed with seismic identified horizons, was imported in the Geosoft, GM-SYS 2D modelling software (Popowski et al., 2009) for magnetic and gravity modelling. The resistivity boundaries in the MT profile were demarcated. The boundaries, together with seismic horizons (where identified), define lithological boundaries or change of rock properties. The demarcated lithologies were assigned with their respective density and susceptibility to fit the observed magnetic and gravity data available along the profile.

2. GEOLOGICAL SETTING

The Masi area is located within the Finnmarksvidda, Norway's largest plateau, at an elevation between 300 and 500 metres above sea level. The project area is within the Early Proterozoic Kautokeino Greenstone Belt (KGB) which is about 40-80 km wide. KGB is located between the Raiseatnu Gneiss Complex (RGC) to the west and the Jer'gul Gneiss Complex (JGC) to the east; these two units form the basement for the KGB (Siedlecka et al., 1985; Olesen & Sandstad, 1993; Solli, 1988).

The area is dominated by NNE-SSW faults, forming 3-4 regional fault zones (Olesen et al., 1992). The main fault zone is the 230 km long Mierujavri-Sværholt Fault Zone (MSFZ) where the postglacial Stuoragurra Fault (SF) lies. Figure 2 shows the location of the project area on the geological map (within rectangle box). From the east, there is the JGC, Gål'denvarri Formation, Masi Formation and Suoluvuobmi Formation to the west.

As reported in the Masi project N-81-4 (Stevenson, 1984): "The Gål'denvarri Formation, which is about 1-1.5 km thick, is the oldest unit of the KGB in the area. The unit is composed of amphibolites (metabasalts) with some associated volcanic breccia. Ultramafic rocks also exist. The quartzites of the Masi Formation (about 0.5 -1 km thick) unconformably overlay the Gål'denvarri Formation. The Masi quartzite, generally classified as feldspathic quartzite, can also contain chrome-bearing mica. At the base there is a conglomerate with pebbles consisting predominantly of granite, gneiss and quartz. The Suoluvuobmi Formation with a thickness of about 1 km is the youngest unit in the area. It contains mainly mafic metavolcanics, amphibolites, mica schists, black schists and also ultramafic rocks occur."
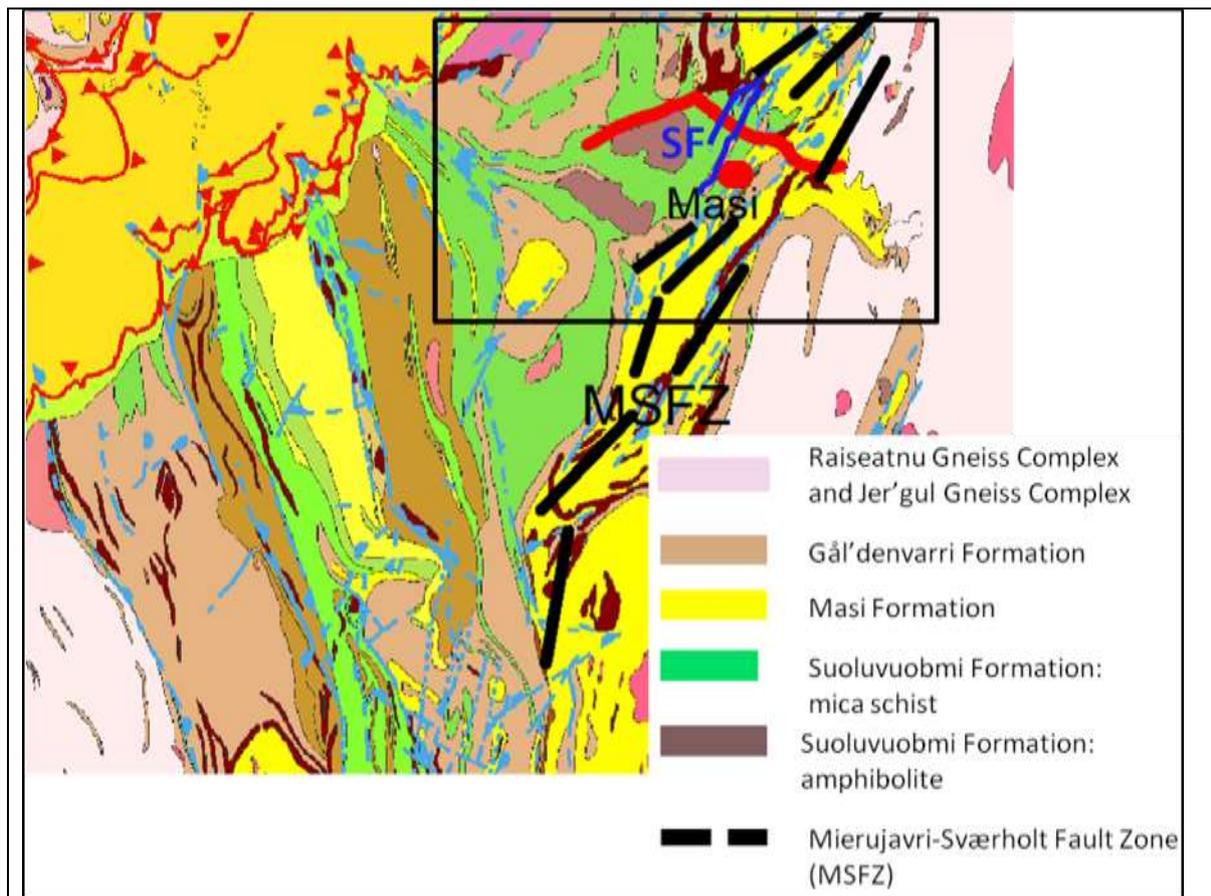
Figure 2: Regional bedrock map of Finnmaksvidda modified after Olesen & Sandstad (1993). The black box highlights the project area and the red line marks the location of the MT profile. The Mierujavri-Sværholt Fault Zone (MSFZ) and the Stuoragurra Fault (SF) are indicated by the black and blue lines respectively.

A regional geophysical investigation using magnetic, CEM and VLF-EM in the Masi area revealed a large regional NW-SE trending conductive body (Stevenson, 1983). Additionally, other localised conductors are present, some of which coincide with a graphite schist horizon and Au-Cu-Pb-Zn bearing zones. Occasional thin sulphide-rich quartz podding was found parallel to, or crosscutting, the schistosity in the amphibolites found in the area (Stevenson, 1983).

3. MAGNETOTELLURIC METHOD

The MagnetoTelluric (MT) method is a passive geophysical exploration technique that measures the Earth's naturally occurring, time varying electromagnetic fields to investigate the subsurface resistivities. Complex interactions between solar wind and the Earth's magnetosphere and ionosphere as well as atmospheric activity are the natural sources for MT. Magnetic fields fluctuate due to these interactions and thus induce currents in the earth (called telluric currents). Earth acts as a good conductor, and therefore induced telluric currents in turn produce a secondary magnetic field. Signal frequencies sensed by MT method are in the range of 10^{-4}-1 Hz from solar wind activity and 1- 10^4 Hz from worldwide thunderstorms (Vozoff, 1991).

MT fields are normally incident on the Earth's surface. These fields travel through the resistive atmosphere as plane waves and penetrate the conductive earth. The plane wave propagation assumption states that the inducing magnetic field only has horizontal components due to large distance to the source (Naidu, 2012). The field propagation becomes diffusive, resulting in the signal attenuation with depth. The attenuation is exponential and also depends on the subsurface conductivity (σ) and angular frequency (ω). The penetration depth can be estimated using a skin depth ($\delta(\omega)$) derivation; the depth at which the signal decays to 1/e of its magnitude at the surface. The skin depth is defined as:

$$\delta(\omega) = \sqrt{\left(\frac{2}{\omega\mu\sigma}\right)} \quad \approx \ 503\sqrt{\rho T} \qquad\qquad \text{Equation 3-1}$$

Assuming the Earth is non-magnetic: $\mu_0 = \mu = 4\pi \times 10^{-7}$ (H/m): vacuum permeability
ω=2πf (Hz)
ρ= 1/σ= resistivity of the material (Ωm)
T= 1/f = period in (s)

The skin-effect states that the penetration of MT fields increases with increasing sounding period, and is low in conductive media and large in resistive environments. Electromagnetic field propagating into the earth (linear, homogeneous and isotropic) has its electric (E) and magnetic (H) field vectors orthogonal to each other (Naidu, 2012). The relationship between the components of the measured E and H gives information regarding the electrical properties of the underlying subsurface. Transformation of the recorded time-series data into frequency domain determine the impedance tensor (**Z**), which is used to derive apparent resistivities and phases at each site as a function of frequency. The relationships between magnetic and electric fields in any medium are described by four Maxwell equations. The book "The Magnetotelluric Method: theory and practice" by Chave & Jones (2012) is recommended for detailed information on the subject.

The impedance tensor (**Z**), also called magnetotelluric response function (Cagniard, 1953) is defined as:

$$Z_{xy} = \frac{E_x}{H_y}$$
Equation 3-2

where E_x is the electric field intensity in volts per meter (V/m) and H_y is the magnetic field intensity in Amperes per meter (A/m).

In a 3-dimensional earth, all the components of the magnetic and electric fields are linked to each other in a matrix form. The impedance tensor **Z** links the corresponding horizontal components:

$$\begin{pmatrix} E_x \\ E_y \end{pmatrix} = \begin{pmatrix} Z_{xx} & Z_{xy} \\ Z_{yx} & Z_{yy} \end{pmatrix} \begin{pmatrix} H_x \\ H_y \end{pmatrix}$$
Equation 3-3

Normally MT measurements for the magnetic fields are done in all three components (x,y,z) while the electric field is measured in the two horizontal directions (x,y), hence **Z** can be computed.

For a 1-D earth, resistivity variations are assumed to be along the z-direction only, thus:

$$Z_{xx} = Z_{yy} = 0 \; ; \; Z_{yx} = -Z_{xy}$$
Equation 3-4

For a 2-D earth, resistivity variations are assumed to be along the z-direction and along one of the horizontal directions (Figure 3). The direction in which resistivity is constant is called a strike direction. MT response is therefore different for electric field polarized across-strike (TM mode) and along-strike (TE mode).
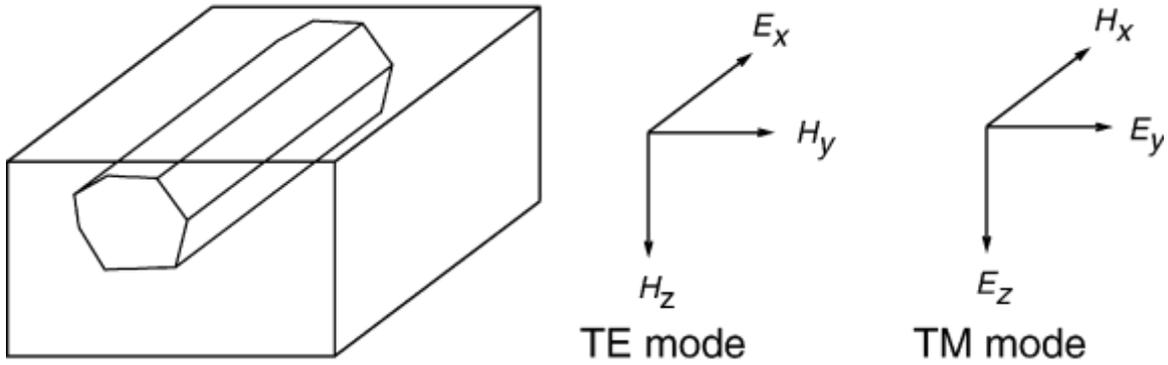
Figure 3: Illustration of a 2D Earth and EM field polarization. The transverse electric (TE) mode is also called E-polarization and Transverse magnetic (TM) is called B-polarization. Image after Unsworth (2007)

Impedance tensor for 2-D earth will be:

$$Z_{xx} = -Z_{yy} \; ; \quad Z_{yx} \neq Z_{xy} \qquad \text{Equation 3-5}$$

For a 2-D Earth with the x- or y-direction aligned along electromagnetic strike, $Z_{xx} = Z_{yy} = 0$.

Apparent Resistivity and impedance phase

Impedence tensor (**Z**) is complex and can be separated into real and imaginary parts. **Z** consists of information about the subsurface apparent resistivity (ρ_a) and impedance phase (Φ). The apparent resistivity and impedance phase are obtained through the amplitude and phase of the impedance tensor respectively.

Apparent resistivity (ρ) is given as:

$$\rho_{xy} = \frac{1}{\omega\mu}|Z_{xy}|^2 \qquad \rho_{yx} = \frac{1}{\omega\mu}|Z_{yx}|^2 \qquad \text{Equation 3-6}$$

For a homogeneous earth, apparent resistivity corresponds to the true resistivity. For a planarly layered earth, the apparent resistivity is some average measure of the resistivities of the layered subsurface. The skin-depth provides some approximate measure of the scale of the inductive volume, which contributes to the surface measurement. In 2D and 3D environments, apparent resistivity representations of the impedance separate into distinct sounding curves and reflect the directional dependencies of subsurface currents. In particular, currents normal and tangential to resistivity contrasts obey different continuity conditions and reflect the effects of charge separations and charge concentrations, respectively.

Impedance phase (φ) is given as:

$$\Phi_{xy} = \arctan\frac{\text{Im}(Z_{xy})}{\text{Re}(Z_{xy})} \qquad \Phi_{yx} = \arctan\frac{\text{Im}(Z_{yx})}{\text{Re}(Z_{yx})} \qquad \text{Equation 3-7}$$

Impedance phase, a phase delay between the electric field (E) and magnetic field components (H) at the earth's surface, relates to the apparent resistivity (Unsworth, 2007) through:

$$\Phi_{xy} = 45 \left(1 + \frac{\partial(\log 10 . \rho_{xy})}{\partial(\log 10 . f)}\right) \qquad \text{Equation 3-8}$$

For a homogenous model, the electric and magnetic fields will have a phase difference of 45° at the surface. Phases are less than 45° if resistivity increases with depth and above 45° if resistivity decreases with depth. As the frequency tends to zero, the apparent resistivity asymptotically approaches the true resistivity of the lower half-

space, and the phase returns to 45°. In a 2D environment, the phases are generally within the 1st and 3rd quadrants; only extreme 2D cases can lead to phase departures out of the quadrant. Out-of-quadrant phases are often observed in 3D environments.

A successful MT survey is based on the simultaneous measurements of both magnetic (H) and induced electric field (E) for each station and a robust low-noise measuring instrument. In addition, source signal strength, duration of survey, presence or absence of coherent and incoherent noise and effectiveness of a robust processing tool will determine the overall data quality.

4. MASI MT DATA ACQUISITION AND PROCESSING

4.1. Survey layout

The survey layout is shown in Figure 4. It is comprised of 40 receiver stations arrayed in a subset of 17 sites in the west, trending NE-SW joining an eastern line of 23 receivers trending NW-SE at an angle of about 130°. The survey layout follows the location of a seismic profile which was acquired in 2012. The overall orientation of the entire profile transverses the general trend of the KGB, which is N-S.
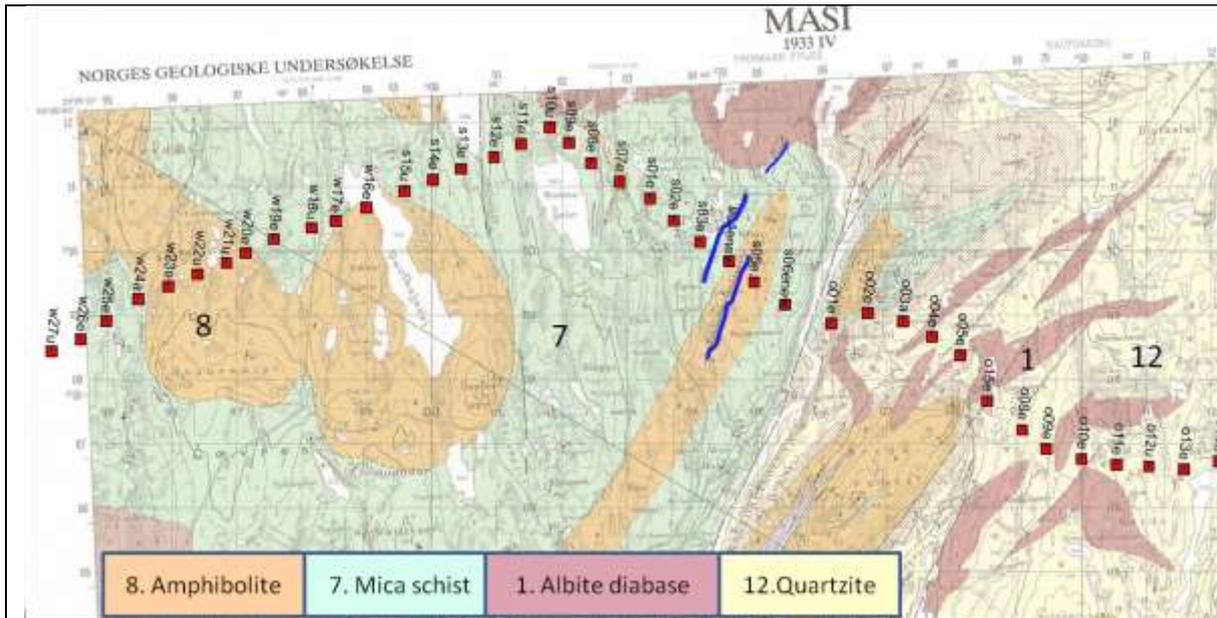
Figure 4: MT Survey layout superimposed on the geological map of the Masi area. Red boxes indicate the MT stations along the profile. Different colours on the map imply different rock types. Dashed lines indicate areas of lithological contacts. The location of the Stuorragurra Fault is highlighted by blue lines.

4.2. Data acquisition

The MT acquisition was carried out from 26.07.2015 to 03.08.2015 and data was collected at 40 stations (Figure 4). Station spacing was about 500 m and recording time of each station was one to two days. Figure 5 highlights the recording times of all stations. MT data was evaluated in the frequency range of 0.001 - 90 Hz (0.01 s - 1000 s).

Three different types of receivers were used to collect this data set (Schmidt, 2016):

1) Analog/Digital Signal Conditioning Units (ADU) – recorded E and H fields
2) Magnetotelluric Units (MTU) from Uppsala University – recorded always E fields, in some cases H fields
3) E-feld Daten Erfasser (EDE) – recorded only E fields

Naming configuration of the receiver stations includes letters in the beginning and at the end to respectively reflect the receiver station along the profile and the type of receiver unit used. First letters: w= west, o= east (øst) and s= south (sør). Last letters: u =MTU, a=ADU and e= EDE
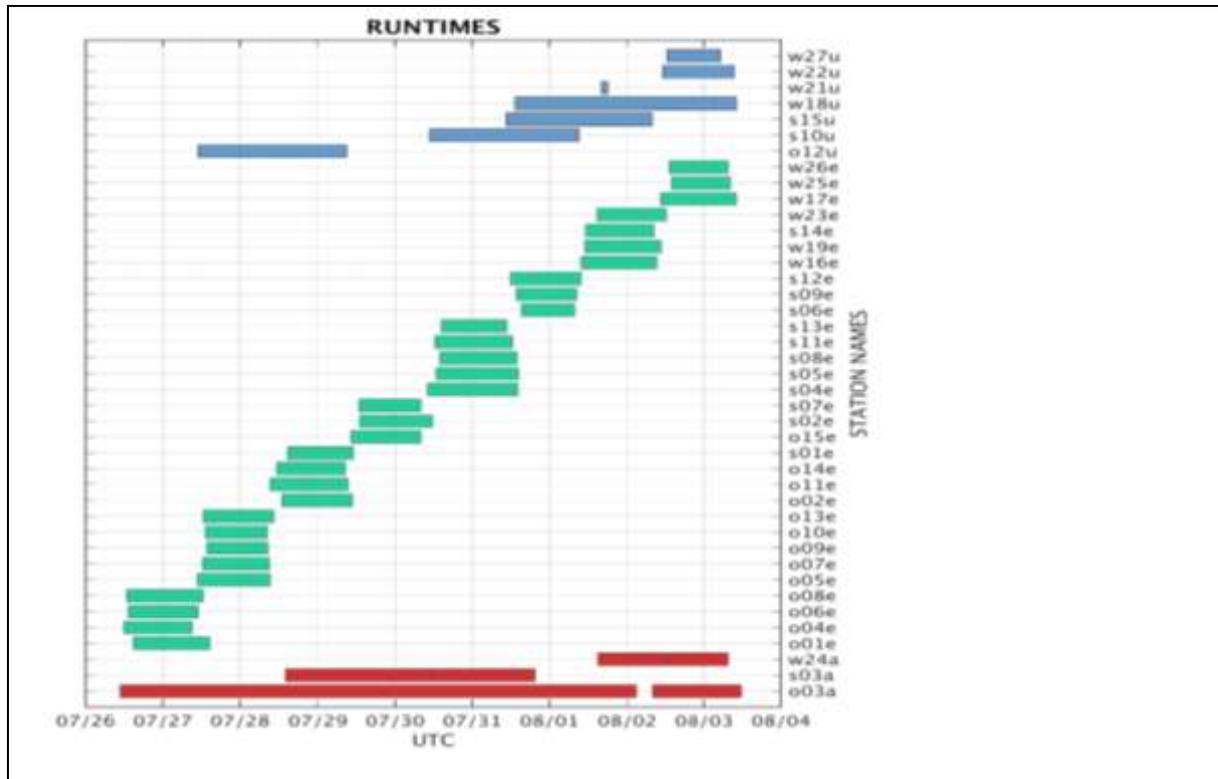
Figure 5: Runtime of the Masi MT stations. Red coloured runtimes are stations that were recorded with an ADU unit, green with an EDE and blue with an MTU unit. The figure is after Schmidt (2016).

4.3. Data processing and assessment

Originally, 44 receiver stations were deployed, of which two were re-deployments (s04enew and s06enew). Stations o06e and o07e had bad quality and hence o15e was deployed to cover the location. Only 40 stations were available for processing. Out of 40 stations available for processing, w21u, s15e and s02e were disregarded because of bad quality.

Data processing was done by Michael Becken at University of Münster using an algorithm based on the robust estimation scheme (Egbert & Booker, 1986). For the processing, local electric fields recorded with telluric-only systems were combined with magnetic fields from a simultaneously recording station equipped with magnetic sensors. These inter-site transfer functions resemble local MT transfer functions but are not identical. Over the spatial scale of the survey, it can be safely assumed that the magnetic source field does not vary. Local anomalous magnetic field variations (e.g. above conductors) can, however, influence the estimates.

However, magnetic field variations are generally small and spatially smooth as opposed to electric field anomalies. Therefore, the exact positioning of magnetic sensors is henceforth disregarded, and inter-site transfer functions are treated as local MT transfer functions as if they would have been recorded at the position of the electric field recorders.

Rotation of the impedance tensor allows for decoupling into the TE (E_x/H_y) and TM (E_y/H_x) modes in 2D environments. For the Masi Survey, stations were laid out such that X components pointed north-south, an assumed geo-strike direction and Y components pointed east-west.

After the time-series data is converted to the frequency domain and the tensor-transfer function is developed, processed data can be visualized in various ways. Figure 6 shows apparent resistivity and phase plots for a few representative stations. Stations from the western part show lower apparent resistivities as compared to those from the central and the eastern parts. Also, all stations show fairly high apparent resistivity values on diagonal components (Z_{xx} and Z_{yy}) of the impedance tensors. This is an indication that the data set is highly affected by 3D resistivity structures. On the other hand, if the coordinate measurements are off the geo-strike, lack of proper rotation required to maximize the TE and TM elements can lead to higher measured values on Z_{xx} and Z_{yy} tensors (Thiel, 2008).
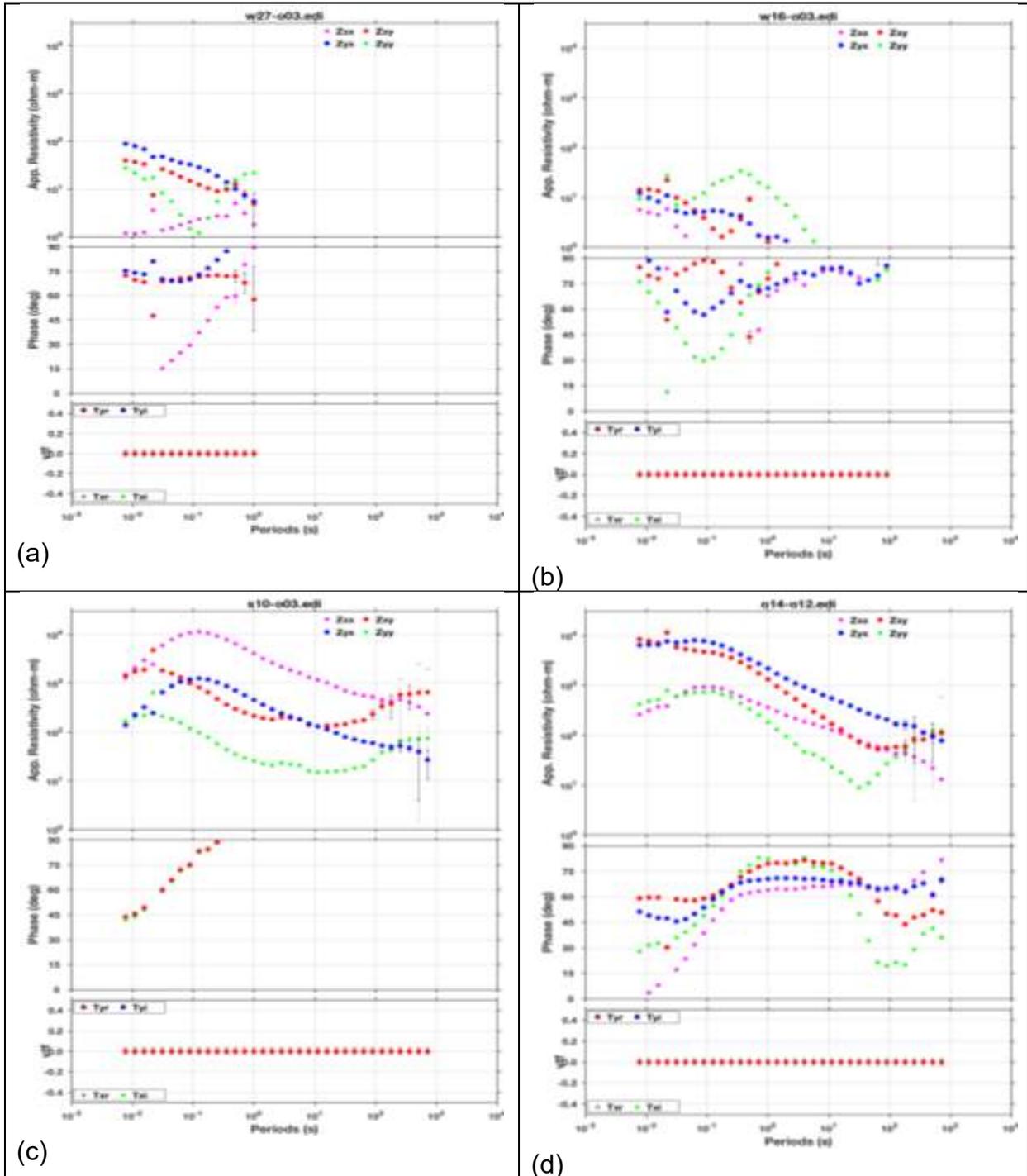
Figure 6: Apparent resistivity and phase plots for stations w27u (a) and s16e (b) from the western side and s10 (c) and o14 (d) from the central and eastern side of the profile, respectively. For each station, the top section shows apparent resistivity as a function of period and bottom section is the corresponding impedance phase. A considerably strong apparent resistivity was measured for the impedance tensors Z_{xx} and Z_{yy} suggesting the data suffers from a 3D effect.

A pseudosection plot is another way of visualizing processed data. In Figure 7, the pseudosection plots display processed data of the 37 stations along the profile. The horizontal axis depicts station positions: the westernmost station w27u to the far left, the s10e at the midpoint (distance 0 km) and the easternmost, o14e to the far right. The data points are displayed as a function of periods in the vertical axis. The plots show a general trend of increasing resistivity towards the east and decreasing

resistivity with increasing periods. However, a number of stations stand out as outliers. These outliers are easily seen in Figure 8; apparent resistivity plots in a grid format. Most of the stations in the western line lack long periods.
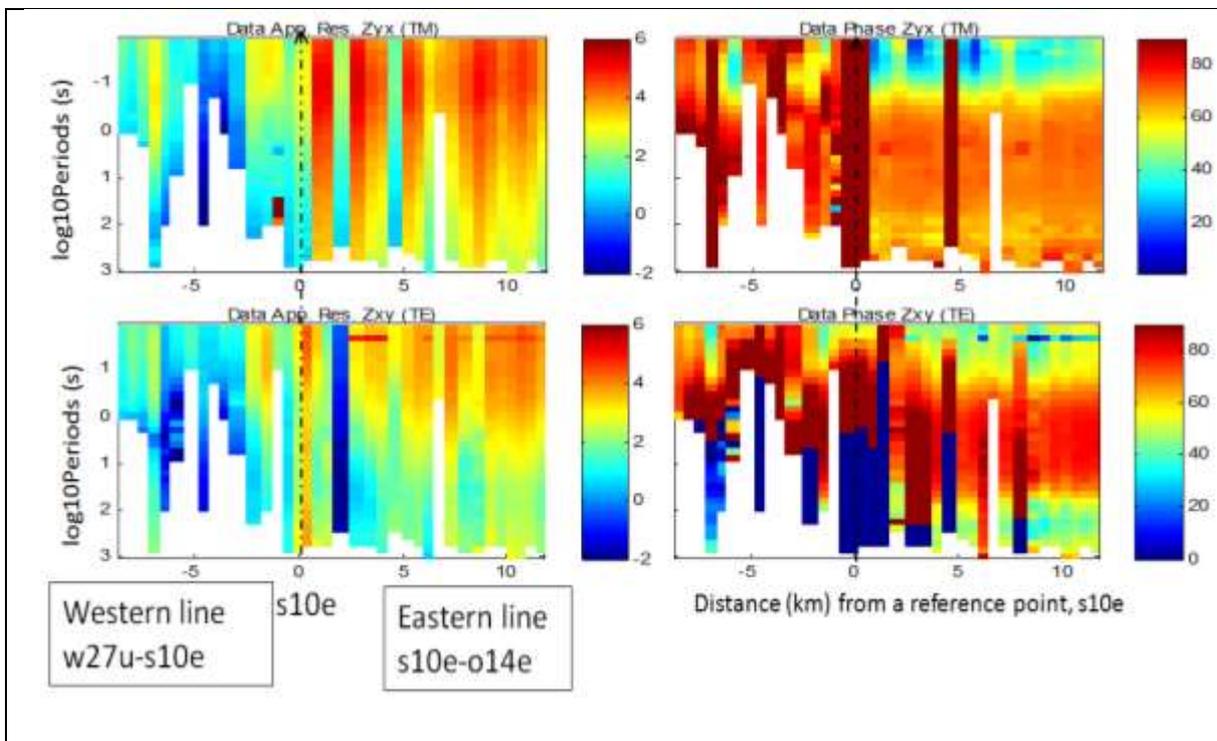
Figure 7: Pseudosection plots of the Masi MT profile. At the top is TM mode and at the bottom is TE mode. To the left is apparent resistivity plots and to the right is corresponding phase plots. The colour bar is resistivity in log scale for the apparent resistivity and degree for the phase plots. A trend of increasing resistivity towards east and decreasing with increasing periods is observed.

Apparent resistivity plots displayed in a grid format (Figure 8) contain the same information as the pseudosections but give a more quantitative assessment. They highlight the trend, geological anomaly and noisy/outliers. However, details of a data point in a single station and also in correlation with neighbouring stations are clearer, not smeared with a colour bar. The purpose of Figure 8 is to inspect individual data points in correlation with other points in the profile; hence the axis values may not be reader-friendly. A general trend of increasing resistivity towards the east is observed. The TM mode (E_y/H_x) displays higher apparent resistivity than the TE mode (E_x/H_y). In general, most stations show impedance phase within the 1st and 3rd quadrant (0° - 90°, 180° - 270°). Some stations have phases out of quadrant, displaying very high values, larger than 90° in the plots. Phases out of quadrant could be due to strong 3D effects or an anisotropic block overlaying another anisotropic layer of a different strike (Thiel, 2008). High phase values are likely impossible to explain by means of 2D modelling and hence they were excluded in inversion.

Observed stations with outliers are:

- Apparent resistivity on stations w26, s09 and s06 (marked with blue dots) show TE and TM modes inconsistent with the neighbouring stations while the phase

data is. This suggests a static shift on either TE or TM modes. The static shift effect is caused by localised resistivity boundaries at a shallow depth.

- Station w24 (marked with a yellow dot) has higher apparent resistivity compared to the neighbouring stations.
- Station s01 (marked with a purple dot) has very low resistivity and could be due to a local conductor in the area.
- Station o08 (marked with a blue dot) shows a high separation on the apparent resistivity but not on phase. This indicates a static shift for one or both modes.
- Stations w19u, w18u, w17u and S11e, s10e, s09e, s07e and s06e (marked with green boxes) display phases out of quadrant

The problematic stations can either be excluded in further processing/inversion or can be improved by reprocessing; in this case they were excluded. Phase points out of quadrant were removed while keeping the good data points.
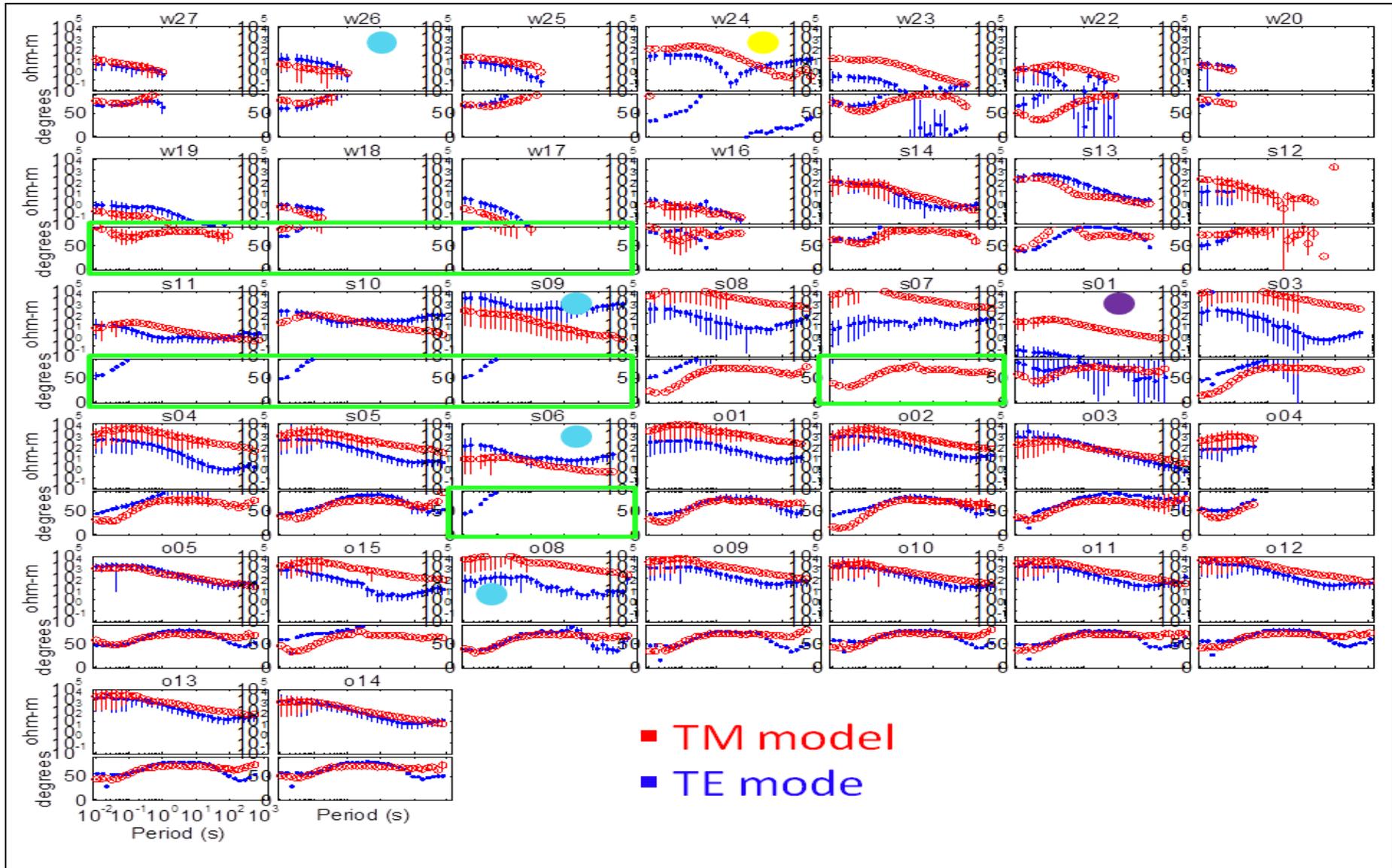
Figure 8: A grid of apparent resistivity and phase plots of the Masi MT profile. Stations are aligned in the order of their position in the profile. From top left is the westernmost station w27u and the bottom last is the easternmost, o14e. Each station in a subplot displays apparent resistivity in the top section and phase at the bottom section. Vertical axes are apparent resistivity (Ωm) in log scale for the apparent resistivity plots and degree for the phase plots. The horizontal axes show periods (s). Phase data for w19u –w17u, s11e –s09e and s06e are out of quadrant.

4.4. MT dimensionality analysis

The assessment of the apparent resistivity and impedance phase suggests strong 3D effects on the data. Understanding the dimensionality is very important for the 2D inversion and the interpretation thereof. We performed dimensionality and distortion analysis by means of the ellipse representation of the impedance tensor (Becken & Burkhardt, 2004).

In a strict 2D environment, it is possible to find a coordinate system in which the two independent MT field polarizations can be expressed by linear polarization states of the impedance columns, i.e. the telluric vectors. Without distortion effect, these principal polarizations are orthogonal to each other and correspond to the strike direction (and the perpendicular direction) of the geo-electrical structure. Galvanic distortion effects can, however, lead to local electric field rotations and thus render the principal polarizations non-orthogonal. In 3D environments, the polarization remains elliptical and no strike can be defined.

In Figure 9, we display the telluric vectors as ellipses in rotated coordinates. The rotation angle is close to zero, i.e. the measurement coordinate system has been maintained. The coordinate system has been defined, however, by the properties of the MT data by minimizing a global measure of ellipticities over all stations and periods. It can be seen from this process that linear polarization states can be found in some survey regions, and in particular within the eastern part of the profile. However, many sites display non-vanishing ellipticities which are indicative of 3D data. Furthermore, ellipses (or linears) are sub-parallel for both principal polarizations for many stations. This suggests strong channelling of the currents, i.e. the polarization direction of the surface electric field is nearly independent on the polarization of the inducing field. Strong conductive contrasts and highly conductive zones are required to explain this property of the data. The ellipse representation can be employed to extract principal impedances and phases. As an example, we display principle phases in Figure 10 together with their polarization properties. Colours depict phase values. Except for station o05, the principal phases are consistent on the eastern line from s11 (profile distance 7 km). The western line depicts, however, scattered phase values together with strong 3D effects.

Based on these findings, it must be acknowledged that the majority of data is affected by 3D effects and influenced by current channelling, making modelling extremely challenging. Given this, no unique strike direction can be defined, and 2D modelling cannot rigorously be justified. Therefore, we use geological knowledge to define the coordinate system of interpretation (i.e. roughly north-south-extended structures) and delete those aspects of the data with strongest 3D effects (e.g. phase out of quadrant, see Figure 9) for 2D modelling and inversion. We emphasize that all 2D models shown later in this report must be treated with care in view of these complications.
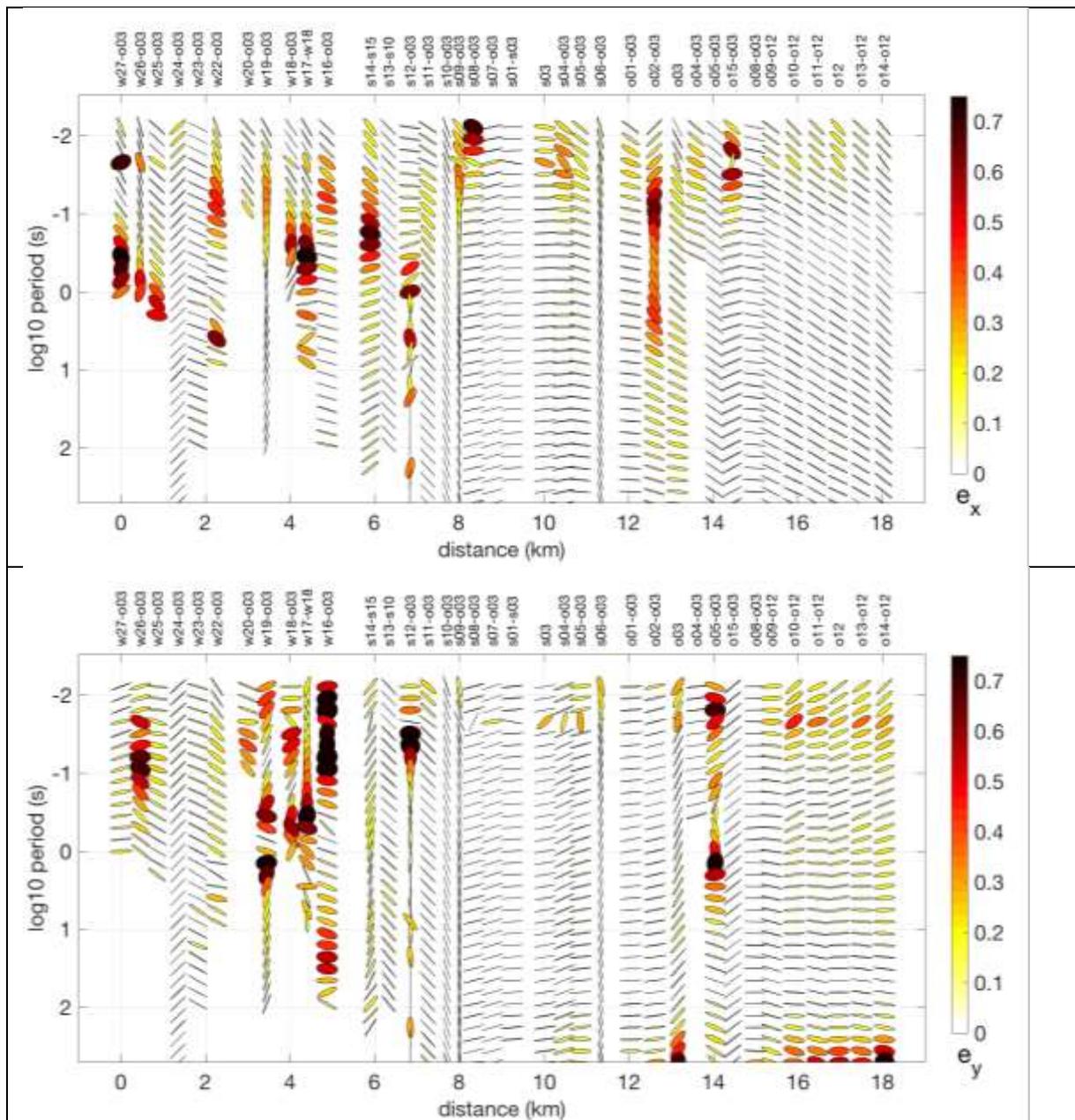
Figure 9: Displays of the telluric vectors as ellipses in rotated coordinates for all periods (vertical axes) and all stations (horizontal axes). The top image is Ex and the bottom is Ey. The colour bar indicates the magnitude of rotation angles. The rotation angles are close to zero suggesting the measurement coordinate system has been maintained.
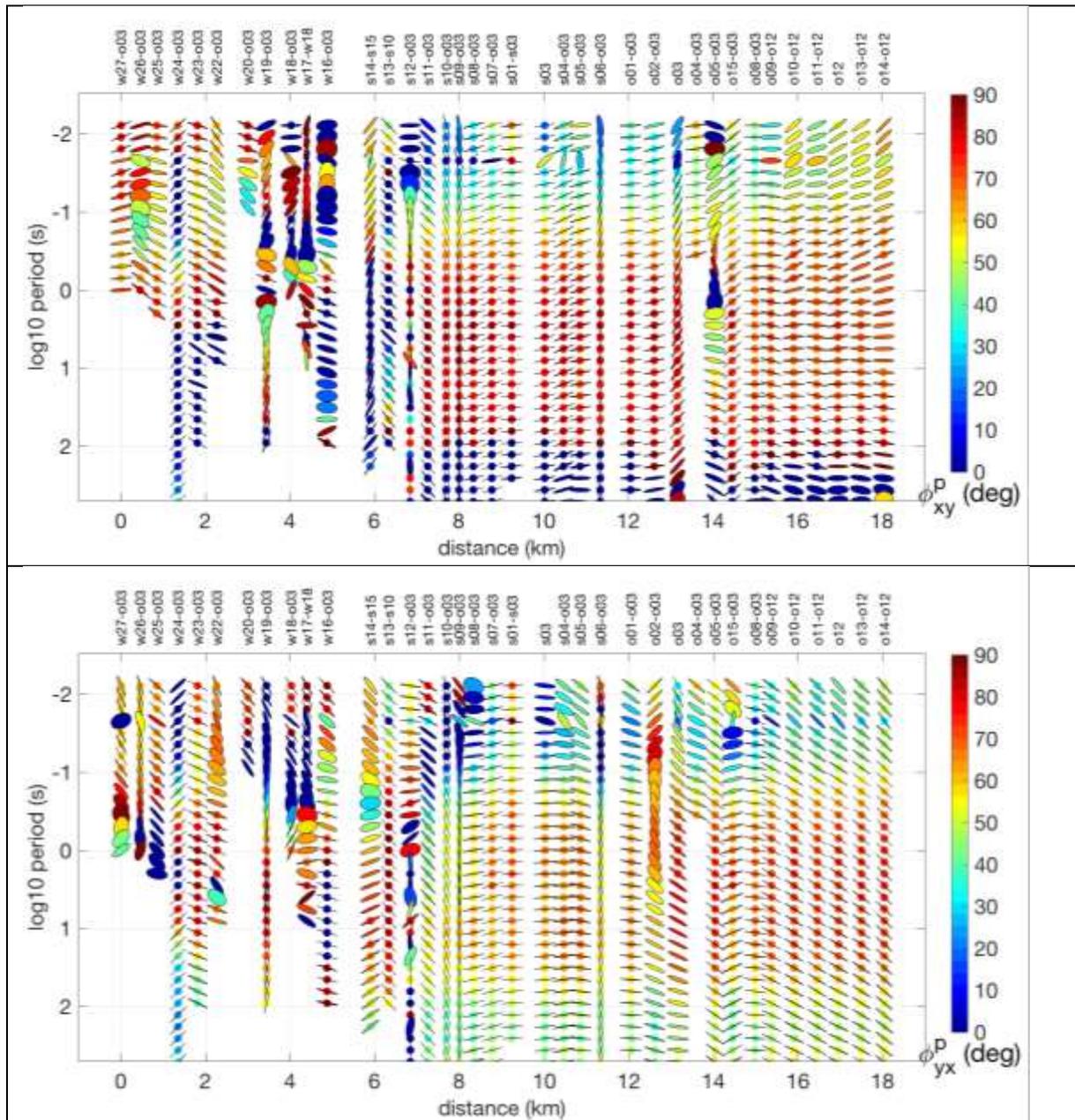
Figure 10: Displays principle phases together with their polarization properties for all periods (vertical axes) and all stations (horizontal axes). The top image is TE mode and the bottom is TM mode. The principal phases are consistent on the eastern line from s11 (profile distance 7 km). The western line shows scattered phase values.

5. REFLECTION SEISMIC DATA ACQUISITION AND PROCESSING

Seismic data at Masi was acquired by the University of Bergen in 2012 along the same profile where MT data was later acquired. The data was acquired using a combination of a snowstreamer and autonomous nodes. The snowstreamer technology (Eiken et al, 1989; Johansen et al, 2011) is an efficient way to do seismic profiling in snow-covered and relatively flat terrain. The seismic source used is detonating cord, which, besides being very efficient and giving a favourable source directivity, has the advantage of leaving no permanent footprint on the ground. The detonating cord was deployed in intervals of 50 m, and each sensor consisted of eight vertical gimballed geophones connected in strings of length 25 m. The seismic data was acquired with 2 ms sampling and 6 seconds recording time. The snowstreamer recorded 60 traces with offsets from 125 to 1625 m. The purpose of the autonomous nodes was mainly to record traces with higher offsets, and to acquire data in areas with rough terrain where the snowstreamer could not be used. The nodes recorded data from the same sources and with the same type of sensors as used for the snowstreamer. Up to 40 nodes were used simultaneously and two geophone strings were connected to each node.

The data processing followed the usual steps for seismic reflection profiling, with trace editing, elevation statics, muting, amplitude corrections, surface consistent deconvolution, and various kinds of filtering and noise reduction techniques followed by velocity analysis, normal moveout corrections and stacking of CMP gathers (traces with a common source-receiver midpoint). In the noise reduction process, velocity filtering (both in the frequency-wavenumber (f-k) and intercept time-ray parameter (tau-p) domains) was used to enhance P-wave reflections while reducing surface waves, S-waves, ambient noise and incoherent energy. P-wave velocities were generally around 6 km/s, except for the upper 100-200 m where the velocity could be down to between 4 and 5 km/s. Migration was also tested, but because the total seismic section is composed of several short line segments, migration artefacts were quite strong.

The migrated seismic profile is shown in Figure 26. Its correlation with the MT resistivity model and the subsequent interpretation is discussed in chapter 9.

6. MARE2DEM MT INVERSION METHOD

MARE2DEM is a parallel adaptive finite element code for 2D forward and inverse modelling of electromagnetic data. MARE2DEM was originally designed for marine controlled-source electromagnetic (CSEM) and marine magnetotelluric applications, but it can also be applied to onshore electromagnetic modelling problems (Key, 2016). It is an open-source code and freely available on http://mare2dem.ucsd.edu/?page_id=108. The code was developed by Kerry Key (Key, 2016).

The model domain is flexibly parameterized using unstructured triangular grids. Arbitrary shapes enable complicated structures such as topography or other horizons to be easily assimilated. MARE2DEM efficiently solves the forward problem in parallel by dividing the input data parameters into smaller subsets using a parallel data decomposition algorithm. The data subsets are then solved in parallel using an automatic adaptive finite element method that iteratively solves the forward problem on successively refined finite element meshes until a specified accuracy tolerance is achieved. Regularized non-linear inversion for isotropic or anisotropic conductivity is accomplished with a new implementation of Occam's method (Constable et al., 1987) referred to as fast-Occam (Key, 2016).

The fast Occam inversion seeks to minimize a cost function (misfit), **U,** of the form

$$U = \|Rm\|^2 + P\|m - m^*\|^2 + \mu^{-1}\|W(d - f(m))\|^2 \qquad \text{Equation 6-1}$$

Where m is the nth dimensional vector of model parameters with units $\log_{10}$ (resistivity), The first term on the right-hand side measures the model's roughness and **R** is the roughness operator.

The second term measures the model's deviation from a prejudice model, **m*** (optional)

The third term is the fit of model's forward response **f(m)** to the observed data vector **d** weighted by the data uncertainties **W**.

The Lagrange multiplier **μ** is used to balance the trade-off between the data fit and the model roughness and model prejudice parameters. It controls how smooth the model will be. High values of **μ** result in a smoother but not well fitted model. It also helps to stabilize the inversion.

The model roughness parameter can be expanded to define all the involved parameters.

$$\|Rm\|^2 = \sum_{i=1}^{m} A_i \left[\sum_{j=1}^{N(i)} wi \left(\frac{\Delta m_{ij}}{\Delta r_{ij}} \right)^2 \right]$$
<div align="right">Equation 6-2</div>

$$\Delta m_{ij} = m_i - m_j$$
<div align="right">Equation 6-3</div>

$$\Delta r_{ij} = \sqrt{\left(\frac{y_i - y_j}{w_{hv}} \right)^2 + \left(z_i - z_j \right)^2}$$
<div align="right">Equation 6-4</div>

$$w_j = \frac{A_j}{\sum_{k=1}^{N(i)} A_k}$$
<div align="right">Equation 6-5</div>

A_i is the area of parameter **i** and accounts for the integration over the parameter region

$N(i)$ is the set of all parameters sharing a vertex with parameter **i**.

m is a vector of model parameters and the term $\left(\frac{\Delta m_{ij}}{\Delta r_{ij}} \right)^2$ approximates the gradient at parameter **i** using an area weighted average of differences between all parameters in a ring surrounding parameter i.

w$_{hv}$ is a horizontal to vertical penalty weight: When $w_{hv} > 1$, it biases the inversion towards enhanced horizontal smoothness, when $w_{hv} < 1$, vertical smoothness is enhanced.

For triaxial anisotropic model, the roughness parameter is redefined as:

$$\|Rm\|^2 \equiv \|Rm_x\|^2 + \|Rm_y\|^2 + \|Rm_z\|^2 + \alpha \|m - m'\|^2$$
<div align="right">Equation 6-6</div>

$$m = \begin{bmatrix} m_x \\ m_y \\ m_z \end{bmatrix}, \qquad m' = \begin{bmatrix} m_y \\ m_z \\ m_x \end{bmatrix}.$$
<div align="right">Equation 6-7</div>

The first three terms on the right side of Equation 5-6 measure the spatial roughness of each anisotropic component while the last term is a measure of the anisotropy.

α is anisotropy penalty weight. It controls the size of the penalty against anisotropy. **α** is in a range of 0 to 1 where 0 is to favour anisotropic models and 1 will favour isotropic models.

7. MT SYNTHETIC EXAMPLES

Before inversion on observed data is performed, forward and inverse modelling is conducted on synthetic data to test the code and build confidence on the results of the observed data. Figure 11 displays the model from which the synthetic data was extracted, added 4% noise and inverted. Station locations and frequencies were based on the observed Masi MT data while resistivities were based on the resistivity logs. A trend of increasing resistivity towards east was inspired by the trend observed on the Masi MT data. A horizon separating 10000 Ωm and 5000 Ωm layers was created from skin depth calculations of the first periods and their respective apparent resistivities of the Masi MT data. A 3000 Ωm, thin layer just below the surface is based on a muted top section of a seismic image available along the Masi profile.
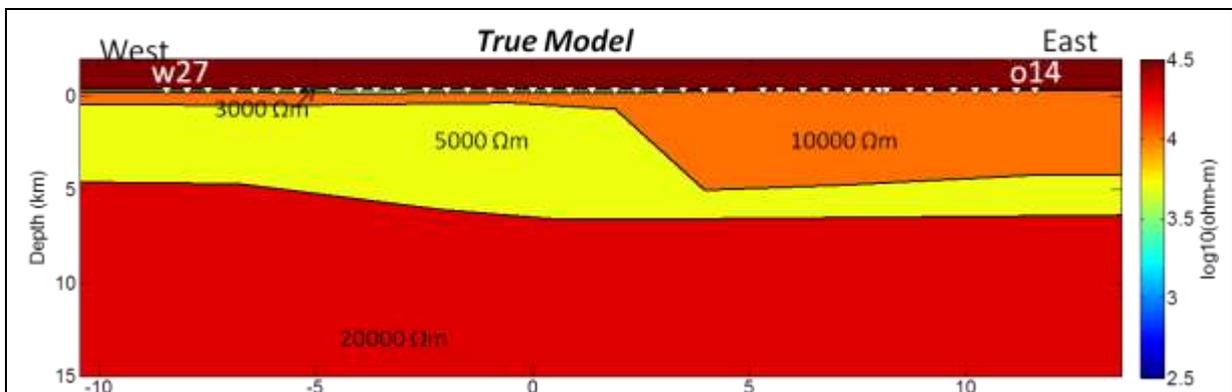
Figure 11: Synthetic model from which the synthetic data was extracted. 42 receiver stations denoted by white triangles are spaced about 500 m apart based on the station spacing at the Masi profile.

7.1. 2D inversion of the synthetic data

A number of inversions were run to test suitable parameters that will give a meaningful model with a low data misfit. Table 1 below summarises the results of different runs tested on joint TE +TM modes. All inversions were set with a target misfit of root mean square (RMS) error of 1. Besides a higher initial misfit, starting models didn't play a big role on the final results. Figure 12 displays the best inverse model based on misfit and visual assessment, inv3. The thin layers (about 200 m and 700 m thick) at the shallow depth to the left were not resolved at their given size and resistivity contrasts.

Table 1: A summary of parameter testing on synthetic data inversion. µ = Lagrange multiplier and Whv =Spatial Horizontal/vertical weight. Parameters Whv =3 and µ =5 gave the best result.

MT mode TE+TM	Half space start model	Whv	µ	Initial Misfit	Final Misfit RMS@iteration	Comments on final models
Inv1	100 Ωm	3	5	53.86	1.58@15	Good results
Inv2	3000 Ωm	3	5	31.32	2.87@7	High RMS error
Inv3	10000 Ωm	3	5	44.99	1.80@15	Good results
Inv4	10000 Ωm	1	5	44.99	2.01@11	Poor results
Inv5	10000 Ωm	0.5	5	44.99	2.30@15	Poor results

| Inv6 | 1000 Ωm | 3 | 2 | 28.66 | 2.87@14 | Artefact to the west |
| Inv7 | 1000 Ωm | 3 | 5 | 28.66 | 1.96@36 | Artefact to the west |
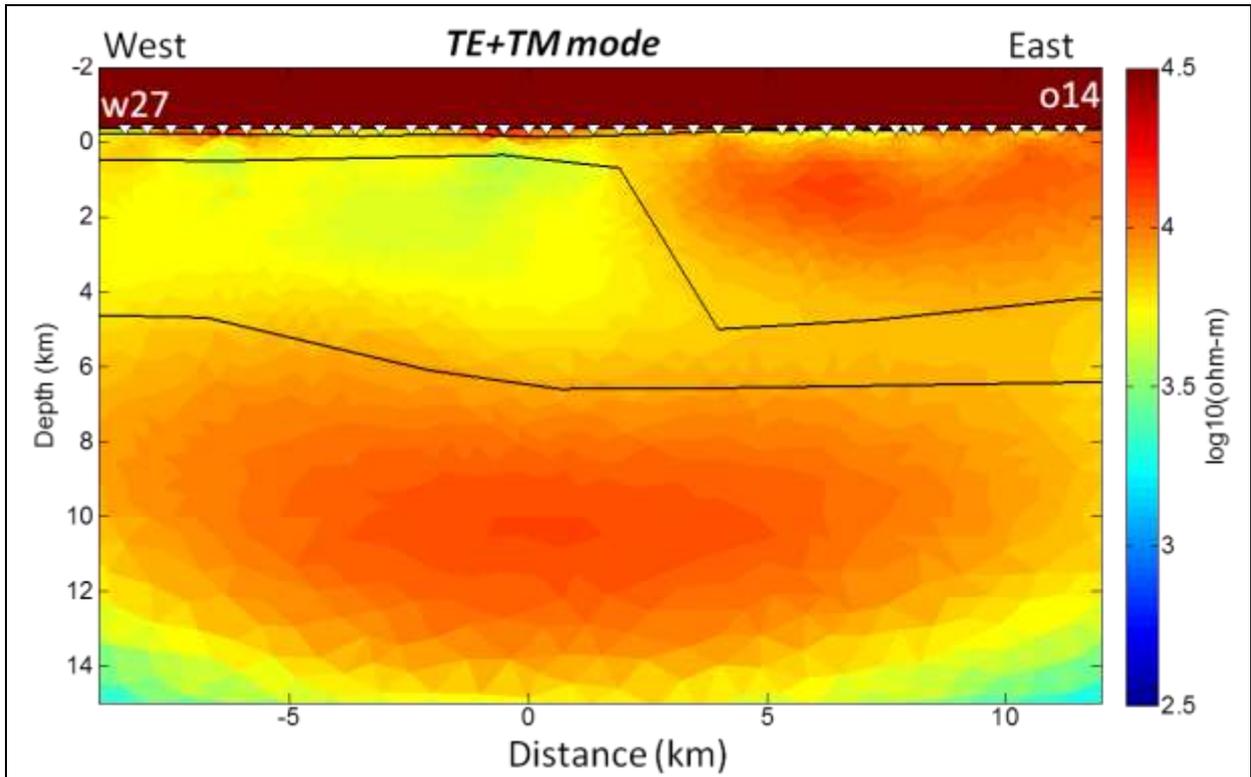
Figure 12: Joint TE+TM inversion result of the synthetic data using Whv=3 and μ=5 and 10000 Ωm half space starting model. Resistivity boundaries are delineated reasonably well. Initial misfit is RMS error 44.99 and final misfit is RMS error 1.8 after 15 iterations.
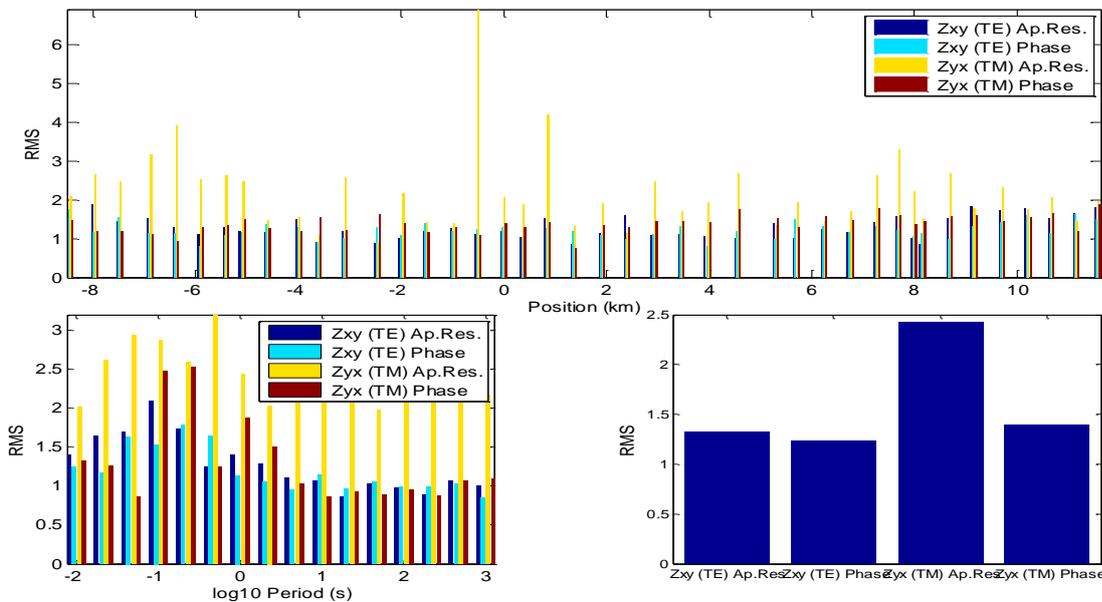
Figure 13: Misfit evaluation of the TE+TM inversion results. Top is misfit for every station for all components. Bottom left is misfit at each period for all components and bottom right is misfit of each component. In general, TM mode apparent resistivity shows a higher misfit.

8. THE MASI MT DATA INVERSION

8.1. Input data

The observed data discussed in Section 4.3 is our input to the MARE2DEM inversion. The data is clear of the outliers (Figure 14). A trend of higher resistivity to the eastern line compared to the western line is observed on all components. Also, resistivity is decreasing with depth. While TE mode shows a general trend, the TM mode in addition, shows some anomalies along the profile. There is a conductor at short periods in the western line named anomaly A. There are two resistive anomalies at the eastern line named B and C.

TM mode is effective in locating resistivity contrasts along the profile. This is because in the TM mode the electric current flows across the boundaries between regions of differing resistivities, which causes electric charges to build up on the interfaces (Unsworth, 2007).
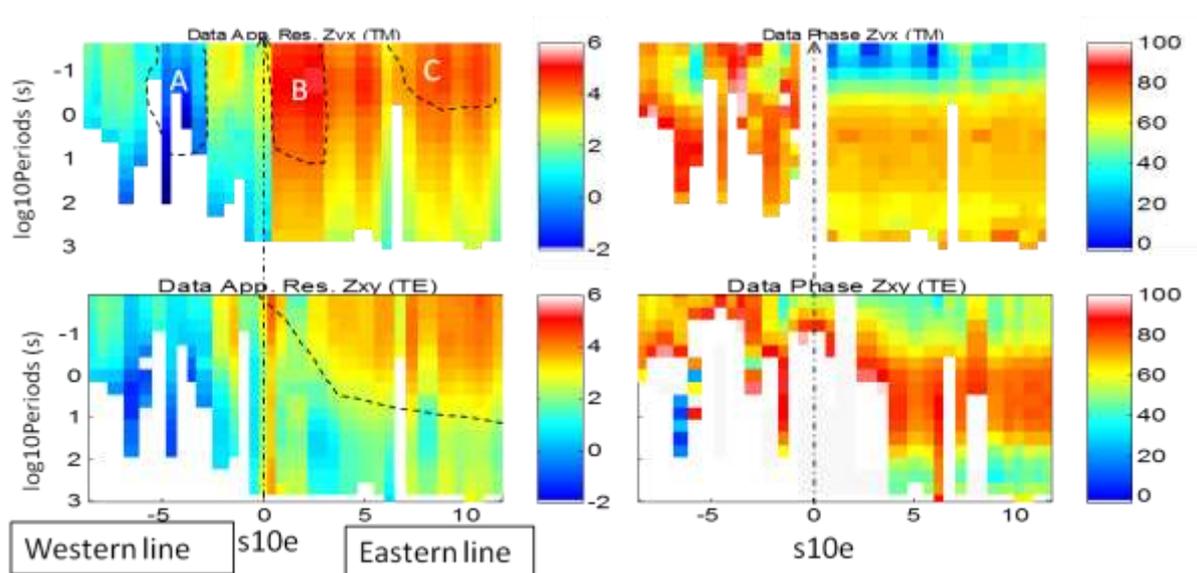
Figure 14: Pseudosection plots of the cleaned MT data input to the inversion. Top is TM mode and bottom is TE mode. To the left is apparent resistivity plots and to the right is corresponding phase plots. The colour bar is resistivity (Ωm) in log scale for the apparent resistivity plots and degree for the phase plots. Station s10e is at the junction of the western line and the eastern line. Letters A, B and C denote the observed anomalies.

8.2. Preliminary inversion results

All model parameters are defined within triangular blocks as shown in a superimposed mesh of the half space starting model in Figure 15. The starting model was set for triaxial anisotropic inversion with resistivity 1000/1000/1000 Ωm for Rho_x/Rho_y/Rho_z components. The air above the topography is fixed to 10^{12} Ωm. At a region down to 1 km below stations and 3 km beyond the last stations, the mesh is denser with a maximum length of 300 m for each block. The maximum length size increases to 600 m down to 3 km deep and 1000 m down to 10 km deep. The outer

box extends to 10 km beyond the last stations and down to 15 km. The maximum length of a block in the outer box was set to 2000 m. Beyond the outer box, the block sizes were set to increase to unlimited size because data sensitivity is also diminishing as going farther beyond the last stations.
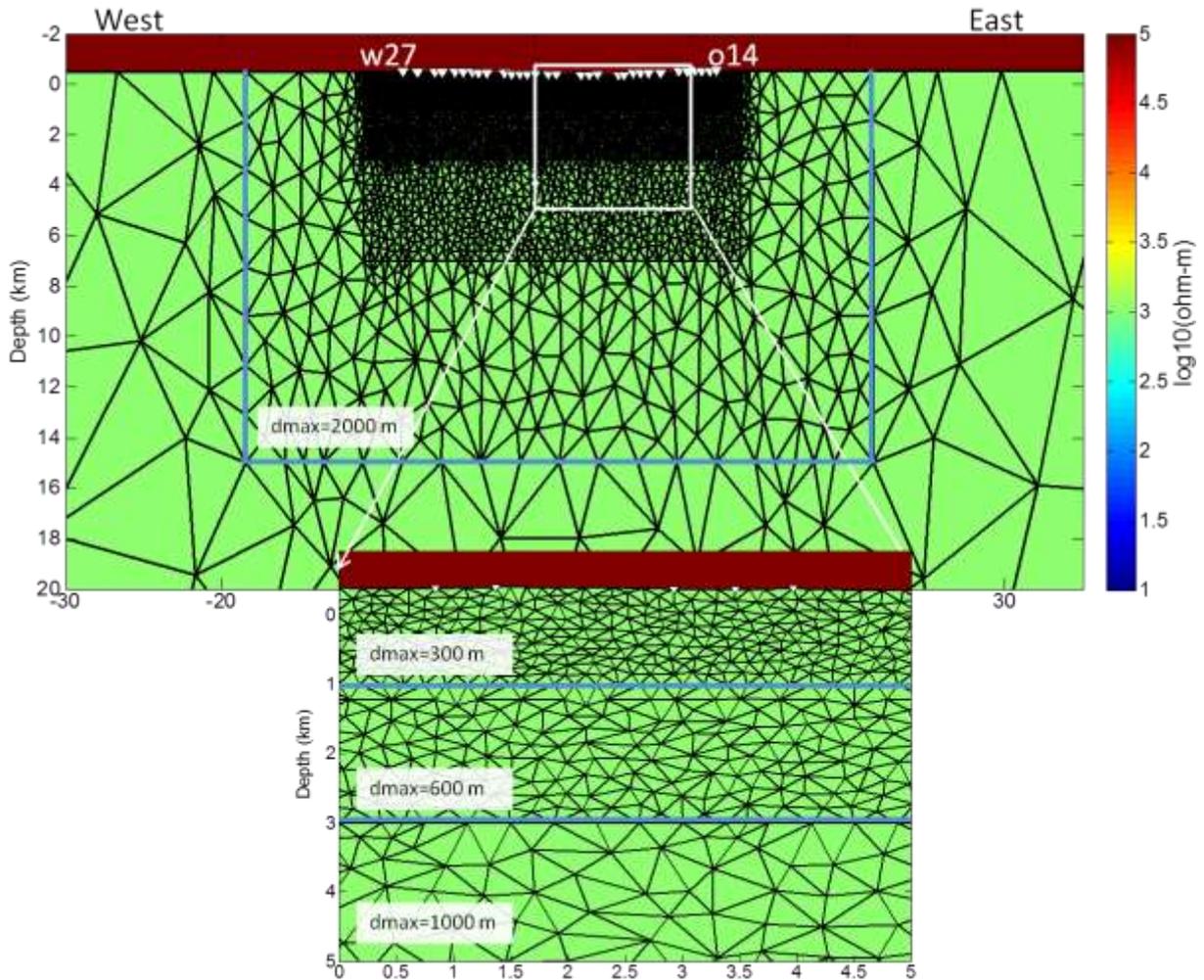
Figure 15: Half space starting model superimposed with inversion mesh (black triangular blocks). The bottom image is a zoomed section of the above model. The white triangles are MT stations.

The preliminary inversion was meant to evaluate the input data. The problematic data points normally show up with extreme misfits. The first attempt was to run inversion using parameters obtained from the synthetic study. However, the inversion did not converge and hence default parameters were used:

- Spatial horizontal/vertical weight (w_{hv}) of 3,
- Lagrange multiplier (μ) of 5 and
- Anisotropy penalty weight (α) of 1

Inversion results based on the half space model are displayed in Figure 16. Inversion was run for the following three cases: only TM mode, only TE mode and joint TE+TM modes. The TE only and the TM only were run with isotropic settings. The joint TE+TM inversion was run with triaxial anisotropic settings. All inversions were set with a target

misfit of RMS error of 1. The TM mode inversion has a starting model misfit of RMS error 19.66 and converged to RMS error 1.94 after 16 iterations. Inversion result of the TE only has an initial misfit of RMS error 7.33 and converged to RMS error 2.52 at iteration 16. The joint TE+TM has initial misfit of RMS error 15.41 and converged to RMS error of 3.04 at iteration 11.
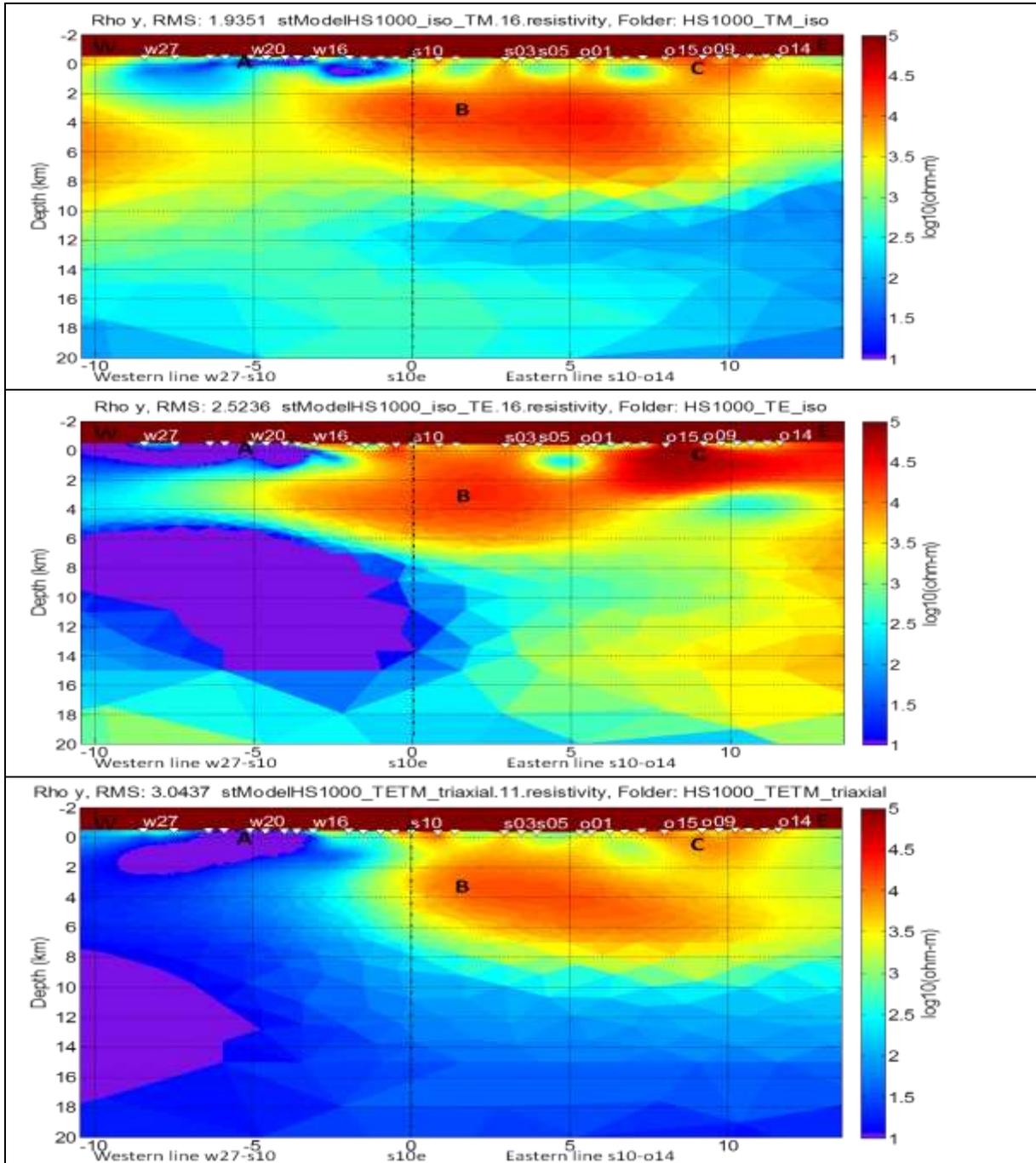
Figure 16: Preliminary inversion results based on 1000 Ωm half space initial model. From top bottom are the TM, TE and joint TE + TM results. Station s10e at 0 km in the x-axis is at the junction of the western line and the eastern line. White triangles are the MT stations.

The trend observed in the input data is reproduced in the inverse models; increasing resistivity towards east and a general decrease at deeper section. A conductive

anomaly at shallow depth to the west and resistive anomalies below the eastern line are also noticeable. A detailed discussion of the observations is given in section 8.4.

The TE data input in the western line have very low apparent resistivity and this is clearly resolved in the inversion. The contribution of the TE mode in the joint inversion is definite. This very low resistivity at depth indicated by the TE but not so pronounced in the TM mode raises a question on whether the data is eligible for 2D inversion. The dimensionality analysis indicated high 3D effects in this section of the profile and hence TE might be highly influenced by the effect.

A synthetic study by Siripunvaraporn et al. (2005), demonstrated that the TM mode is least affected by 3D effects as compared to the TE mode. Inversion of only TM mode generates reasonable models. TM mode has a better recovery of structures; however, it tends to underestimate the true resistivity contrast.

In general, the differences of Z_{xy} and Z_{yx} can be significant. Therefore, joint TE+TM inversion often helps to retrieve the most realistic model. In this case TE mode is deemed to be highly affected by 3D effects, therefore not fit for 2D assumption. Since TE mode is not good, joint inversion will not be helpful either.

In the following sections only the results of TM mode inversion will be shown and discussed.

8.3. Testing of the starting models and inversion parameters

In the previous section we show preliminary results of an inversion run using default parameters. To optimise the results, different parameters and starting models were tested to get the best model explaining the Masi MT data. Results of the different tests are shown in Appendix A. Different starting models are observed to converge towards similar final results.

A priori information about the area indicates the presence of faults and lithological contacts across the profile. A spatial horizontal/vertical weight (w_{hv}) of 1 and a Lagrange multiplier (μ) of 2 were the trade-off parameters to a converging inversion. w_{hv} = 1 favours the vertical and horizontal smoothing equally, hence accounts for both horizontal and vertical structures along the profile.

In the synthetic study (Section 7), w_{hv} = 3 which favours horizontal smoothing gave good results. This is due to the absence of vertical structures in the synthetic model. The observed (real) data, however, is from a fractured and faulted geology. A test of w_{hv} = 3 resulted in smoothening away the faulted sections of the model (Appendix A).

8.4. Final inversion results

The final inversion applied a half space starting model (Figure 17). The starting model was set for isotropic inversion with a resistivity of 2000 Ωm. The mesh setting is similar to that in Section 8.2. As concluded from parameter testing. Inversion was run with a spatial horizontal/vertical weight (w_{hv}) of 1 and a Lagrange multiplier (μ) of 2.
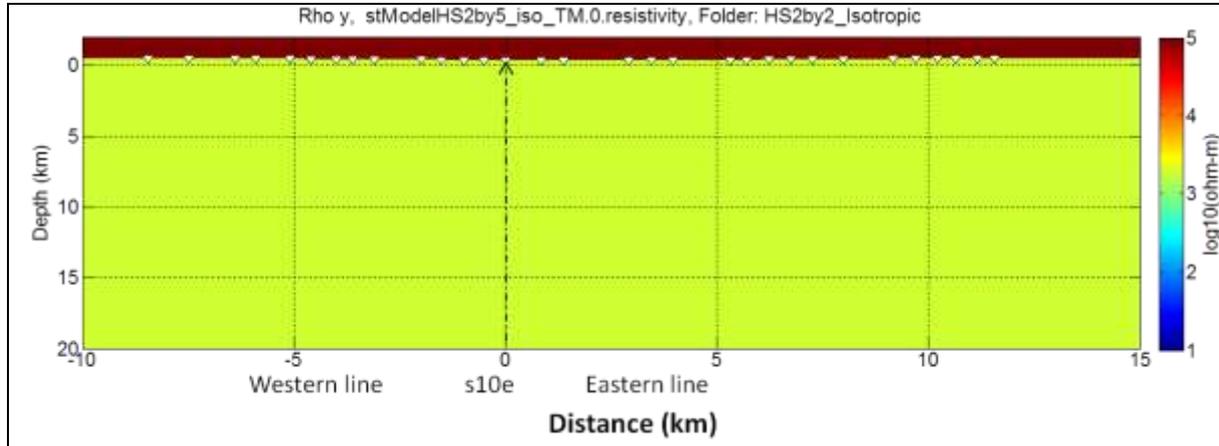
Figure 17: Half space starting model used in the final inversion. Station s10e at 0 km in the x-axis is at the junction of the western line and the eastern line. White triangles at the top are MT stations.

The final model of the isotropic inversion is shown in Figure 18. The model indicates a general background of increasing resistivity towards east and a decrease at depth. The low-resistive zone (about 250 Ωm) to the west hosts a conductive anomaly A (10-100 Ωm). The shallow subsurface to the east shows an alternating resistivity pattern (650-8000 Ωm). It is in this section where anomaly C is located (8000 Ωm). Below the two zones is a region of a relatively high resistivity background (about 6000 Ωm) and the anomalous body B (up to 33000 Ωm) is observed in its central part. Underlying the resistive layer is a low-resistive region (100-400 Ωm) which becomes shallower towards east. The inverse model reproduces the trends observed in the input data.

A dense receiver spacing (500 m) and higher frequencies of up to 90 Hz have been of significance in enhancing imaging resolution for the structures at the shallow subsurface.
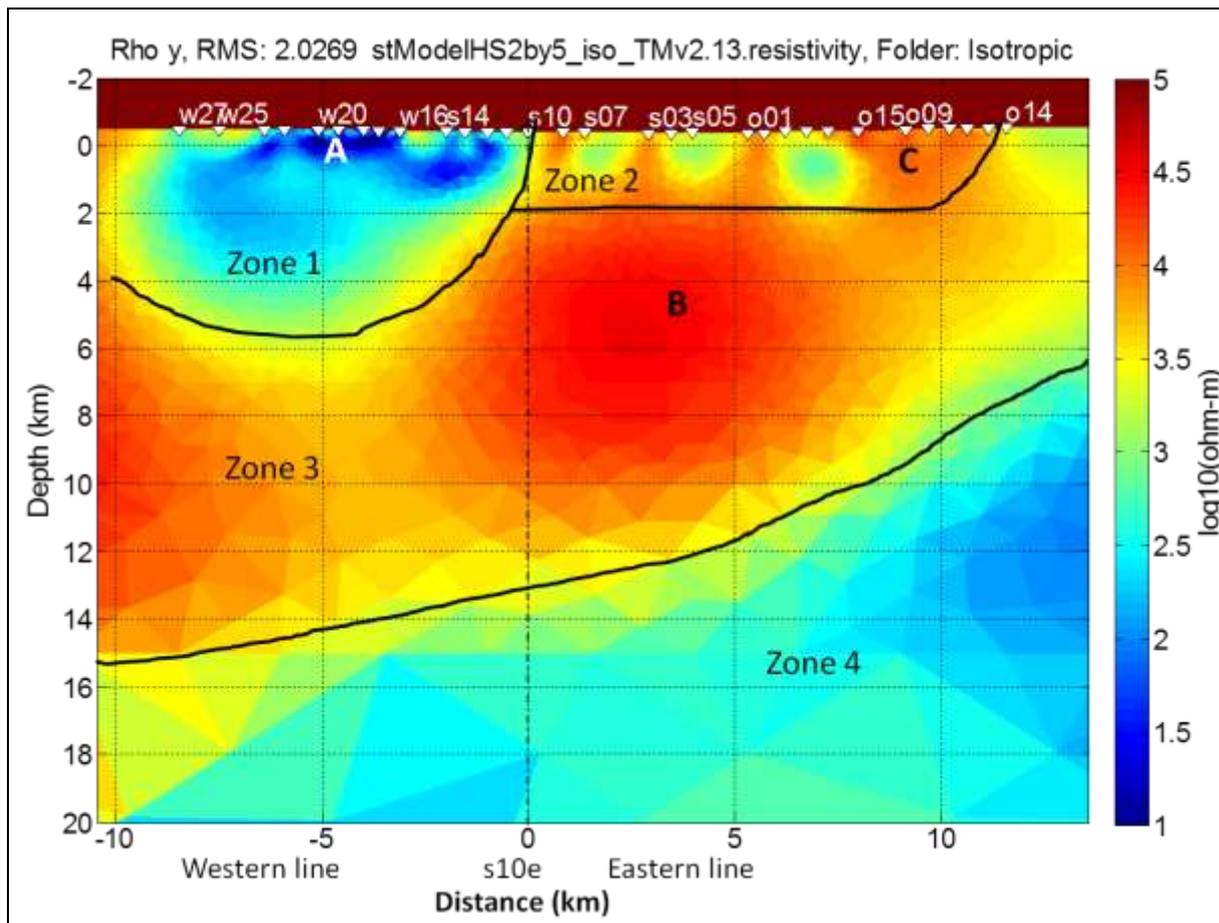
Figure 18: Final isotropic inversion results of the Masi profile down to 20 km deep. X-axis is a distance in km from a reference point, station s10e. The reference point (at 0 km) is at the junction of the western line (left) and the eastern line (right). White triangles at the top are the MT stations; w27u represent the last station to the west and o14 is the last to the east.

Figure 19 shows the inverse model down to 3 km depth for a closer look at the shallow subsurface. Anomalies labelled A, B and C in the input data correlate with the observed anomalies in the inverse model. In addition, there are conductive anomalies standing out of the general resistive background in the eastern line. These anomalies are observed from the surface down to 1.5-2.0 km depth at stations s08 (to the left of s07) to o15 (between 1.4 km and 8 km in the x-axis).
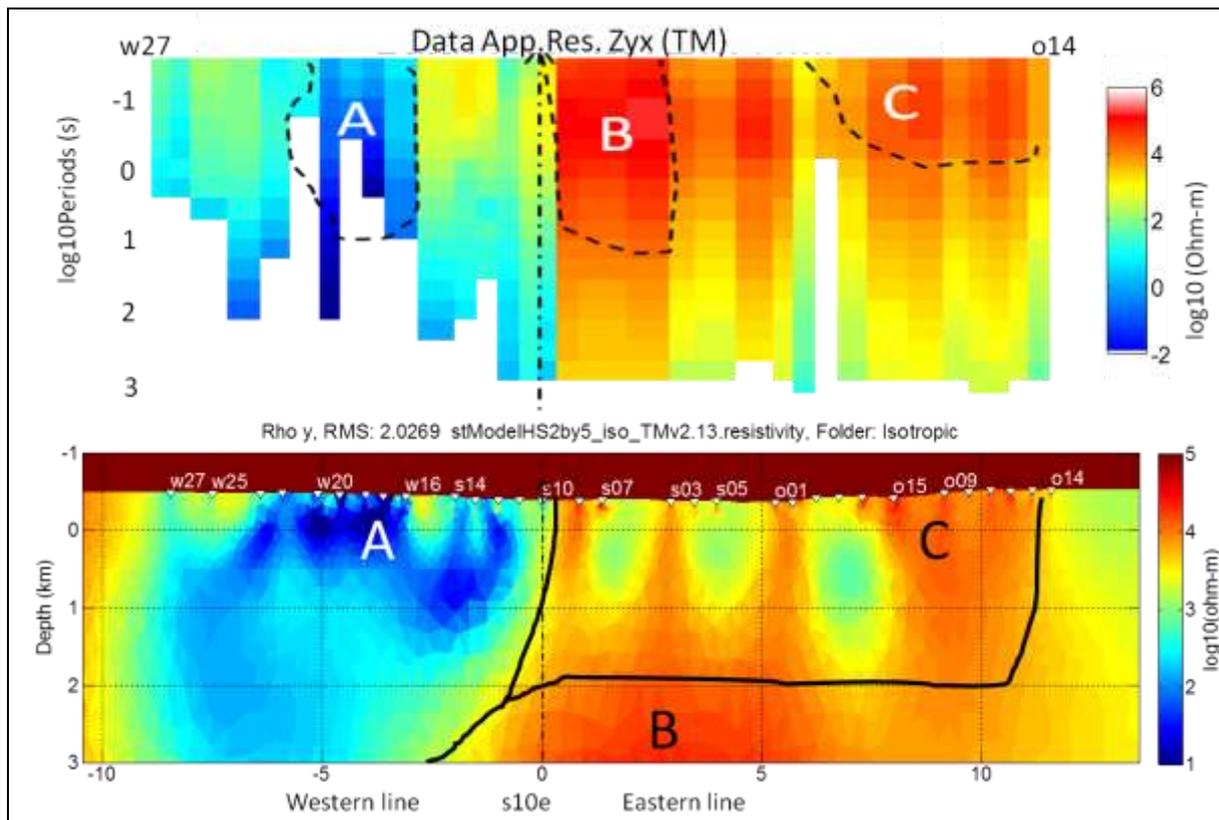
Figure 19: Final isotropic inverse model of the Masi profile down to 3 km depth (bottom) is displayed together with the input data (top). The inverse model is in depth (km) displaying true resistivity (Ωm). The input data points show apparent resistivity (Ωm) at different periods (y-axis). In addition to anomalies A, B and C, the inverse model shows conductive anomalies between s08 and o15.

8.5. Misfit analysis

The data misfit is defined as the RMS error of the difference between the observed (input) and calculated (synthetic) values weighted by the data uncertainty (see equation 6-1 in section 5). The half space starting model had an initial RMS error of 21.2 and converged to RMS error 2.03 at iteration 13. Figure 20 shows the misfit convergence plot. Figure 21 and Figure 22 break down the misfit by components and by data points respectively. In general, the misfit is good.
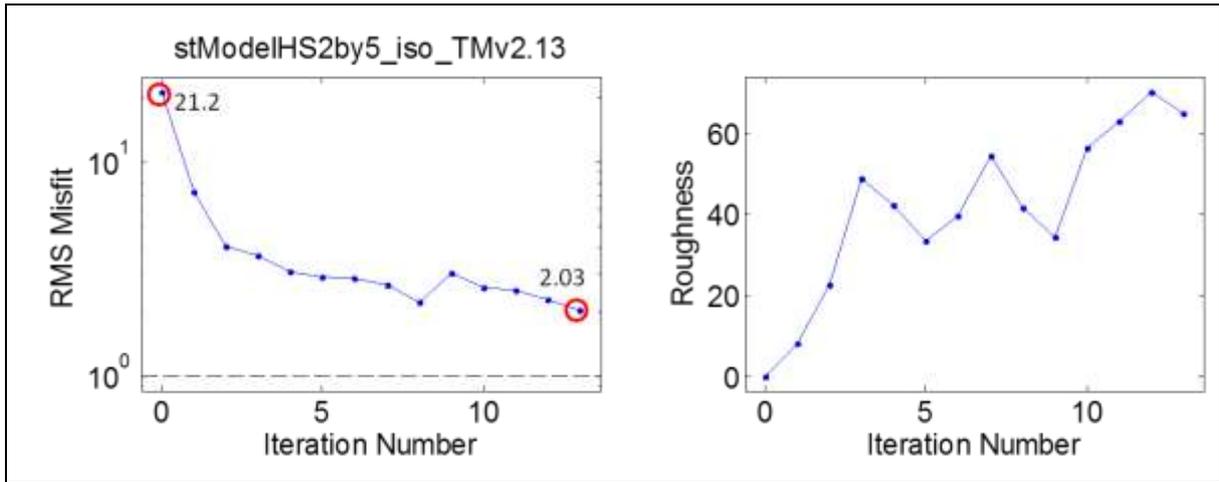
Figure 20: Misfit convergence curve (left) showing average misfit at different iterations. The initial misfit dropped by more than 60% at first iteration and converged to RMS error of 2.03 at iteration 11. To the right is a roughness plot. The model started smoothly but added in structures as the number of iterations increased
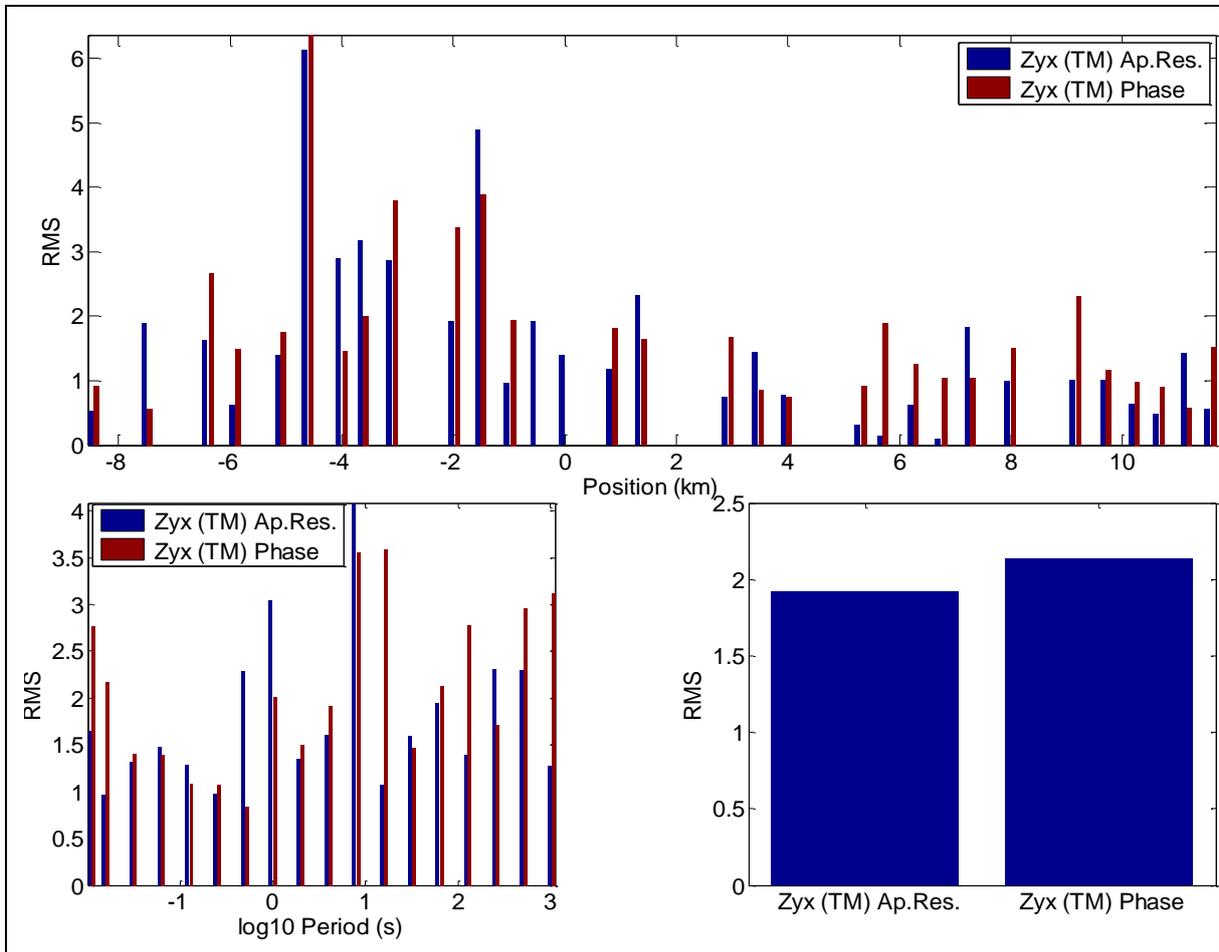
Figure 21: Misfit breakdown plot showing average misfit for apparent resistivity and phase components. The top image is misfit for all stations. At position 0 km (s10e) is the joint between the western and the eastern lines. The misfit is higher at the western line especially the phase data at w19e, the 6th station from left. The bottom left is misfit analysis by periods. The bottom right is average misfit by component, the impedance phase has higher misfit than the apparent resistivity.
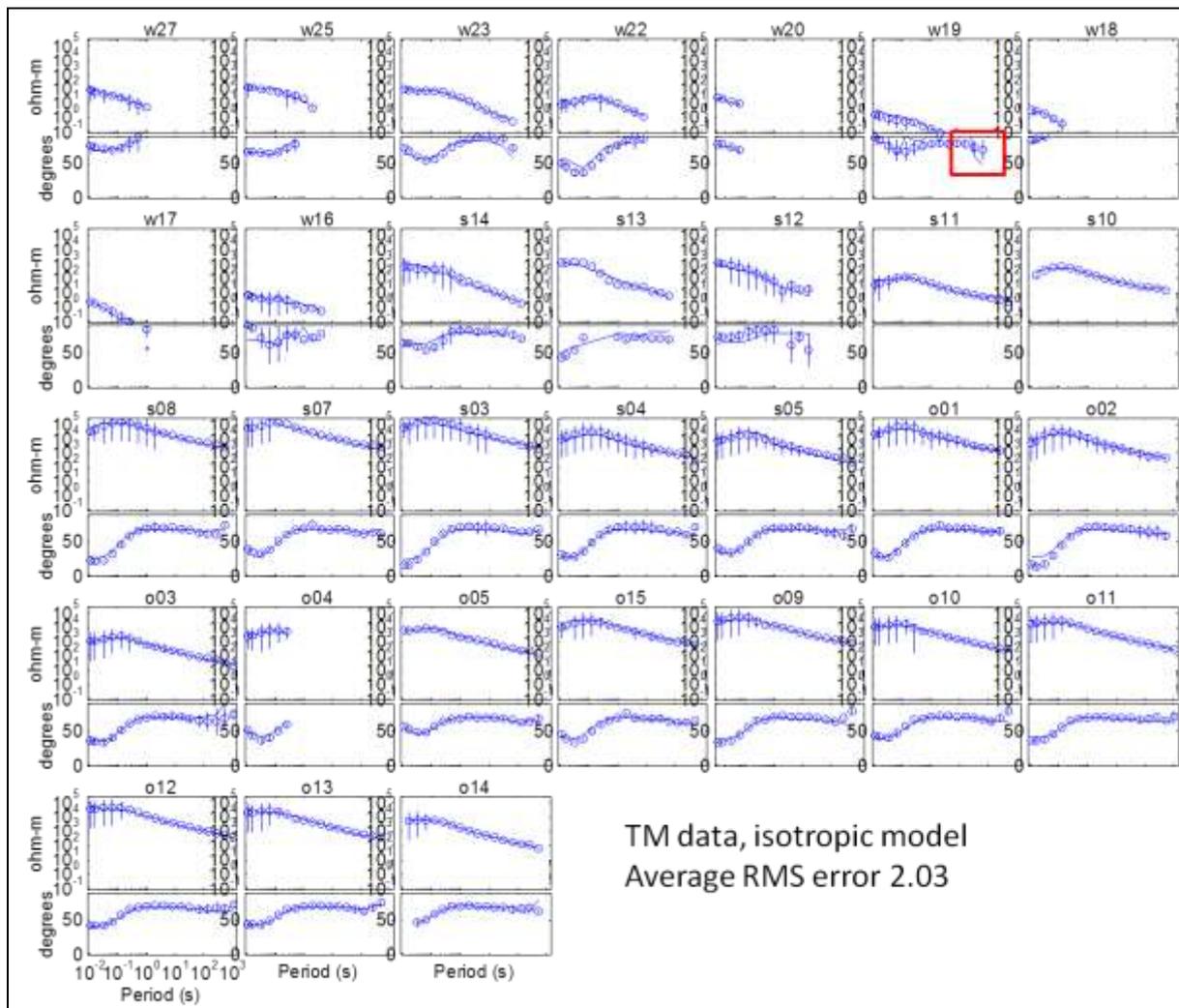
Figure 22: Misfit analysis of the apparent resistivity and phase curves of input data (circles) and synthetic values (lines). Station names are on top of each sub-image. Station w19 shows higher misfit marked in the red box. All other stations show a general good fit, within error bars.

8.6. Inversion results: Western and eastern lines inverted separately

The western and eastern lines are joined at station s10e. The lines are joined at an angle, about 130°. To qualify the results of the entire profile inverted on a 2D assumption, the two lines were also inverted separately. The results are shown on Figure 23.

The starting model for the western line has resistivity of 500 Ωm and that of the eastern line has a resistivity of 2000 Ωm similar to the starting model of the entire profile. The target misfit for both lines is an RMS error of 1.0. The starting RMS error for the western line is 27.85 and converged to RMS error 3.15 at iteration 8. The starting RMS error for the eastern line is 10.85 and converged to RMS error 1.08 at iteration 17.
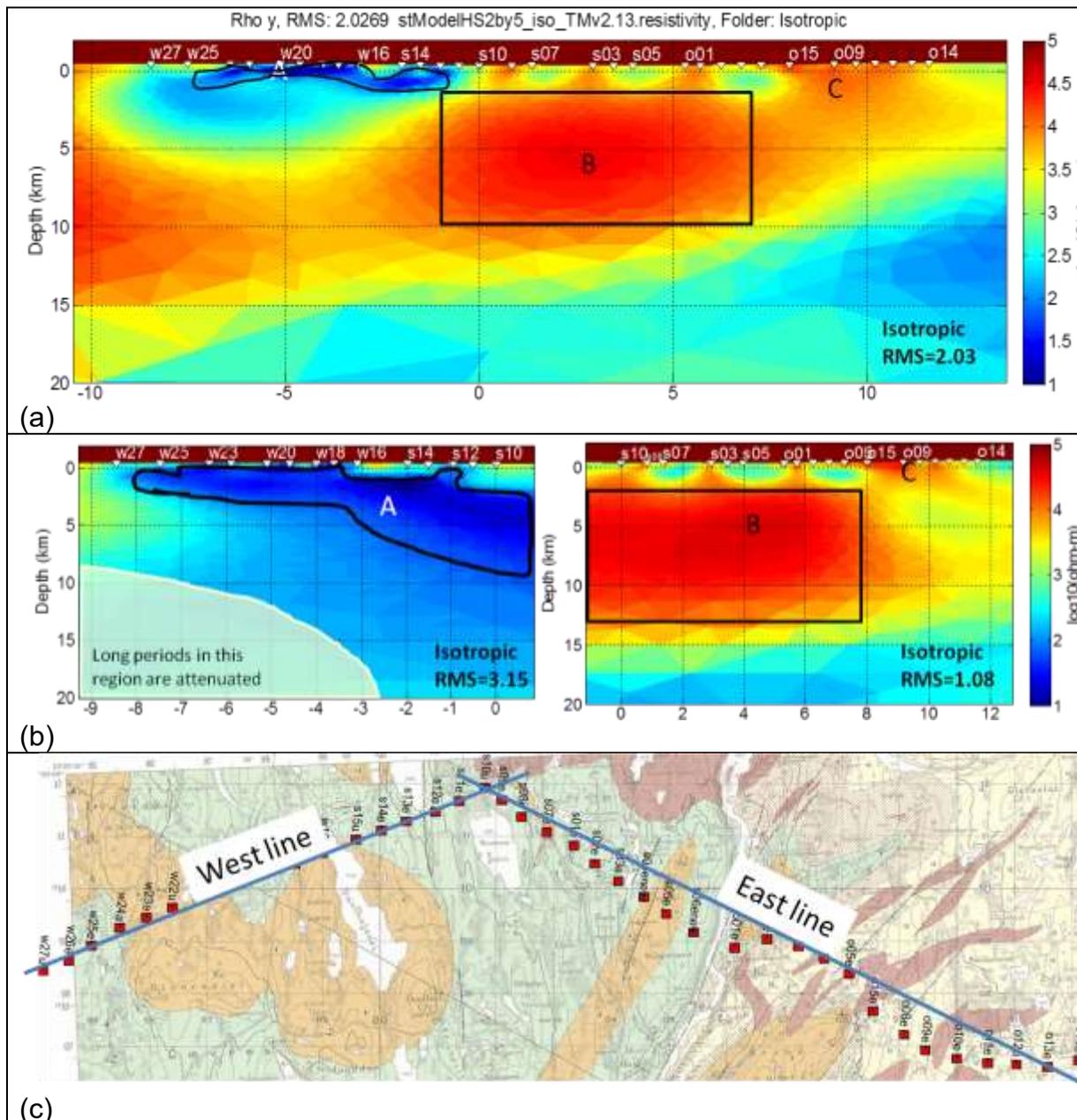
Figure 23: Final inversion results of the Masi profile inverted separately (b). Profiles at the middle left is the western line and the middle right is the eastern line. The top image is inverse model of the entire profile. Station s10 is included in the inversions of all scenarios. The results are slightly different especially on the western line. The locations of the profiles are depicted in the bottom image (c).

The results of the separate lines are as expected from the input data: low resistivity to the west and high to the east. However, they are slightly different compared to the results of the whole data set inverted together. Anomalies A and B extend to larger depths when the lines are inverted separately. The continuous resistive body dipping to the west (Figure 23, a) is not imaged in the western line. The differences are most likely due to:

- Long periods at the western line are mostly attenuated. Sensitivity to the deeper subsurface is impaired.
- Stations from the conductive side (west) and the resistive side (east) which have no association otherwise if inverted separately are made spatially closer when

43

inverting them together in the entire line model. This affects the resistivity distribution along the profile especially at the deeper section.

- At station s10, the low resistivity in the western line and high in the eastern line is explained by misfit analysis (Figure 24). The resistivity in the western line is underestimated.
- Line orientations (Figure 23, c). Based on the structures on the bedrock map, the line orientations are transversing the geo-strike orientations, but the TM mode (of the data) is east-west oriented. Inverting the entire line is a better approximation of the east-west oriented TM mode. For a better comparison, it would be interesting to look at inversion results of the in-line electric (ILE) and cross-line electric (CLE) modes of each line. ILE and CLE correspond to horizontal electric fields rotated along the line and across the line respectively.
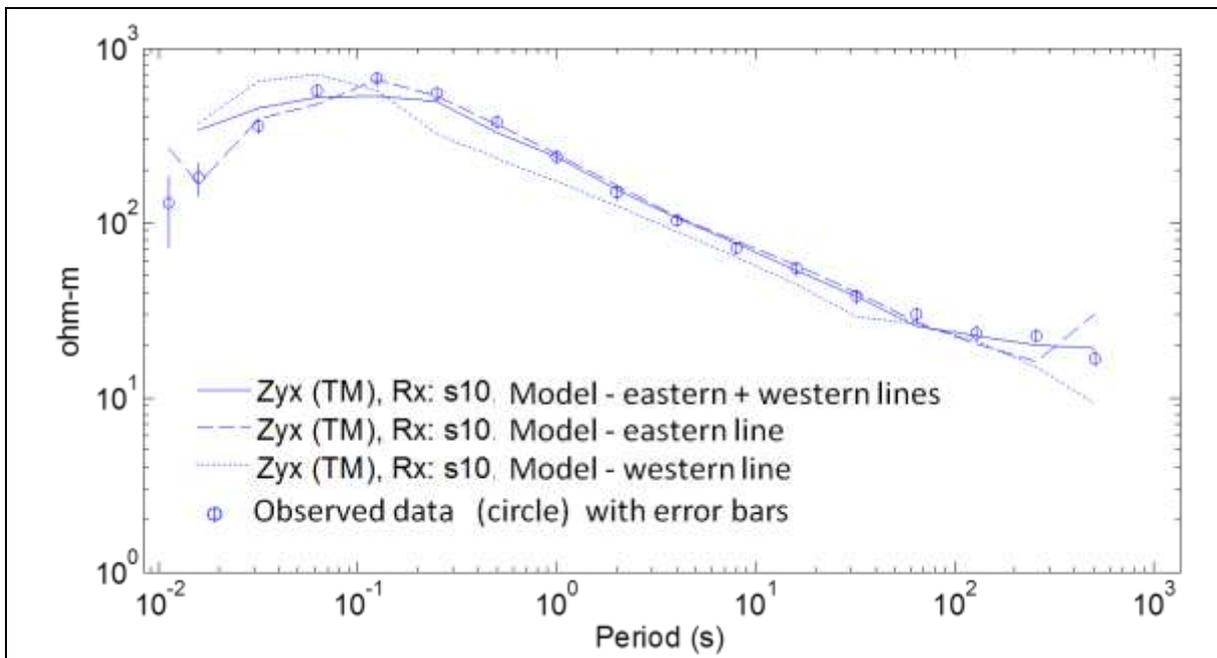
Figure 24: Misfit analysis of the apparent resistivity of the input data (circles) and the synthetic values of station s10 from the three inversion scenarios. The phase data was out of quadrant and hence excluded in the inversions. In general, the solid line (entire line) and the dashed line (eastern line) show a good fit, mostly within error bars. The western line (doted) shows overestimated resistivity in the shallow subsurface (short periods) and underestimated from the middle to deep subsurface (mid to long periods).

9. DATA INTEGRATION AND JOINT INTERPRETATION

The MT method detects variations in the electrical properties of rock units, in particular electrical resistivity. By its nature, MT measures horizontal resistivity and therefore it is a good tool in mapping regional variations in resistivity. It is neither sensitive to thin horizontal bodies nor to small features. Depending on the frequency range, higher frequencies enhance resolution at the shallow subsurface while lower frequencies have a deep penetration capacity to image the deeper subsurface.

Variations in the subsurface resistivity can be due to varying rock types, mineral content, change in fluid content, porosity and the presence or absence of interconnected fractures. At greater depths, higher subsurface temperatures reduce rock resistivities. By visual inspection of the MT inverse model, we see resistivity variations with depth and across the profile. Complementing information from other geophysical and geological data helps to label the resistivity units with lithological names. Along the Masi MT profile, there is a 2D seismic profile from 2012 (chapter 0). Furthermore, both magnetic and gravity data is available along the MT profile. Also, there is a resistivity well log and 2D resistivity profiles (DC) from the nearby areas. Site locations of these data sets are shown on Figure 25.

Figure 25: A map of the Masi area showing the location of the MT and seismic profiles (red line), 2D resistivity profiles (black circles) and the resistivity borehole log (purple circle). From the MT project area, Vuottasjavri is about 10 km, Fiednajohka is about 24 km and Riednajavre is about 81 km away.

As an initial step, a seismic image is superimposed on the MT model for correlation of resistivity boundaries with significant seismic reflectors for interpretation. Also, the resistivity measurements from the well log and 2D profiles are compared to the resistivities of the MT inverse model for correlation. By integrating the bedrock map, the shallow subsurface is interpreted. The bedrock map provides the lithological

contacts at the surface. Below the surface, lithological boundaries were guided by the resistivity boundaries, seismic reflectors (where available), together with density and susceptibility, to fit the gravity and magnetic data respectively. This is how the final interpreted model along the Masi profile was achieved.

9.1. MT model in combination with seismic data

Seismic reflection profiles will mainly show contacts between layers of contrasting acoustic impedance, which is the product of seismic velocity and density. Fractures in rocks will lower the velocities so that fault zones can also sometimes be seen. In order to produce clear reflections, it is necessary for the interfaces to have a sufficient horizontal extent and to be relatively flat. Of the rock types exposed along the Masi seismic line, amphibolite and diabase are expected to have a higher acoustic impedance than mica schist and quartzite, and contacts between those rock types may therefore generate prominent reflections.

The seismic profile is shown in Figure 26. The data was acquired along the same profile as the MT profile, Figure 25. The vertical muted area is where the profile crosses the river, between stations s06 and o01, and there is no data coverage in the area. In general, the image quality is not good. However, a few reflectors are observed. A shallow reflector (h1) at about 200-450 m depth, just below the muted section is noticeable. The reflector can be followed from west at station w27 to s05 in the central part of the profile. This reflector corresponds to the resistivity boundary in the MT model, seen especially in the western part between w23 and s16. Below station s03 there are two east dipping reflectors (SF) which partly correlate with the resistivity boundary at the location of the postglacial Stuoragurra Fault. Another horizontal reflector (h3) is observed in the western part at about 1000 m depth and correlates with a resistivity boundary; the base of the very low-resistive unit. An east-dipping reflector, h5, correlates with the resistivity change at about 1500 m depth below stations o02 – o05. Reflectors h6 and the remaining reflectors do not have a strong correlation with resistivity changes in the MT model. This could be due to lack of resolution in the MT imaging. Thin layers or low resistivity contrast between adjacent layers pose a challenge in MT. The other reason could be that the reflectors are artefacts. The migrated seismic section suffers from artefacts (migration 'smiles') created at the edges of the available data. The section is composed of three shorter sections migrated separately; thus, the migration artefacts cover large parts of the total section.

Figure 27 shows a time domain seismic section. The section is clearer than the depth migrated section but only few reflectors are identified. The wavy reflectors observed in the depth section are therefore interpreted as migration 'smiles'.

In general, only few reflectors have been identified in the seismic section. The MT resistivity model provides more details as complementary information for what is not visible on the seismic image.
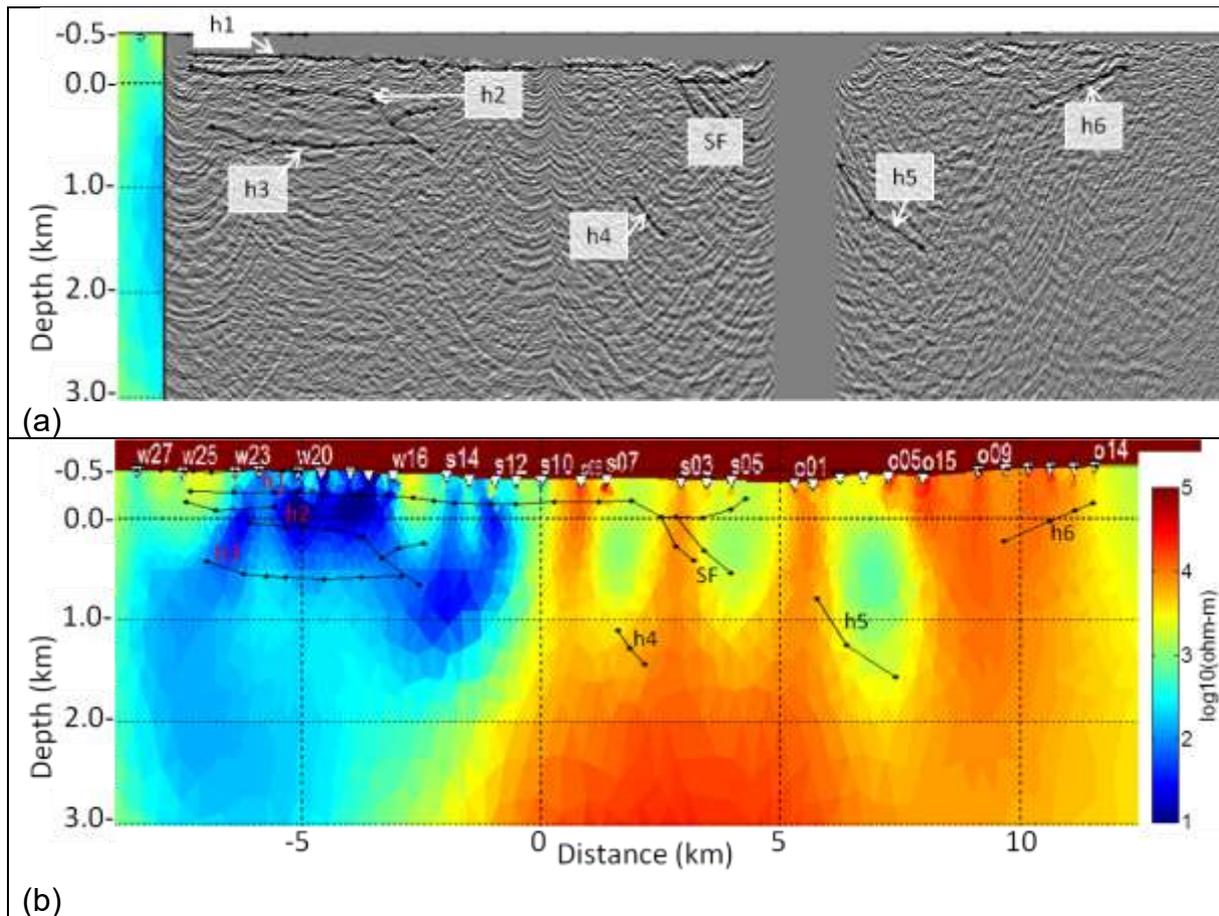
Figure 26: The seismic depth section (a) superimposed on the MT profile. Some of the identified reflectors (h1, h3, h5 and SF) partially or fully correlate with resistivity boundaries in the MT model (b) whereas the rest do not.
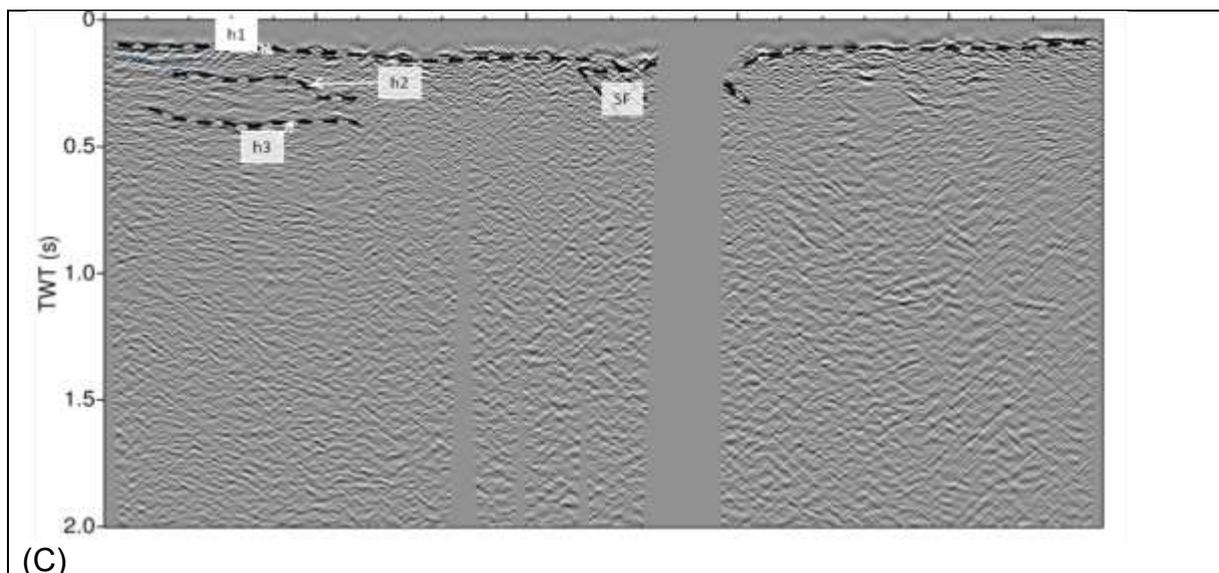
Figure 27: The seismic time section overlaid by some of the identified reflectors from the depth-migrated seismic data. The image is clearer than the depth migrated section, but only few reflectors are matched in the time section. This could mean that the velocity model enhanced some reflectors and/or introduced artefacts in the depth migrated data.

9.2. MT model in correlation with a borehole resistivity log

A 600 m deep resistivity log is available from a borehole at Vuottasjavri, Kautokeino (see Figure 25). The well location is about 10 km to the southeast of the easternmost MT station 014e.
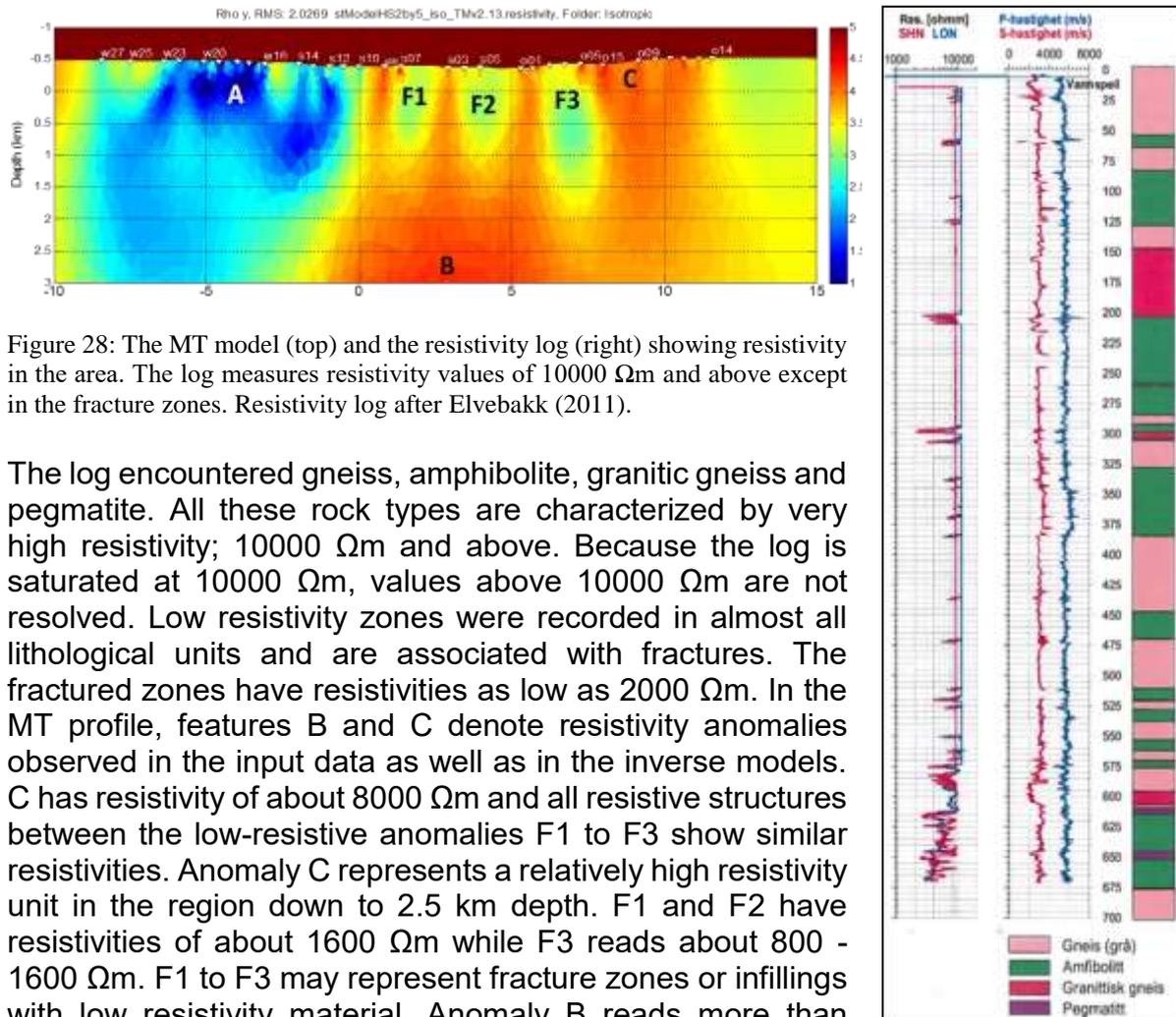
Figure 28: The MT model (top) and the resistivity log (right) showing resistivity in the area. The log measures resistivity values of 10000 Ωm and above except in the fracture zones. Resistivity log after Elvebakk (2011).

The log encountered gneiss, amphibolite, granitic gneiss and pegmatite. All these rock types are characterized by very high resistivity; 10000 Ωm and above. Because the log is saturated at 10000 Ωm, values above 10000 Ωm are not resolved. Low resistivity zones were recorded in almost all lithological units and are associated with fractures. The fractured zones have resistivities as low as 2000 Ωm. In the MT profile, features B and C denote resistivity anomalies observed in the input data as well as in the inverse models. C has resistivity of about 8000 Ωm and all resistive structures between the low-resistive anomalies F1 to F3 show similar resistivities. Anomaly C represents a relatively high resistivity unit in the region down to 2.5 km depth. F1 and F2 have resistivities of about 1600 Ωm while F3 reads about 800 - 1600 Ωm. F1 to F3 may represent fracture zones or infillings with low resistivity material. Anomaly B reads more than 20000 Ωm.

9.3. MT model in correlation with a geological map

Figure 29 shows a geological map of the Masi area. The map shows mica schist and amphibolites (Suoluvuobmi Formation) dominating the central and western area while quartzite (Masi Formation) and albite diabase dominates the eastern area. Anomaly A correlates with the amphibolite outcrops mapped in the area. On the map, the Stuoragurra Fault (SF) is shown between stations s03 and s05 (blue lines on the map). On the MT model this area (F2) is characterized by relatively low resistivity. F2 is about 2 km wide and 1.5 km deep. The older and more regional Mierujavri-Sværholt Fault Zone (MSFZ, thick black lines) is indicated to cross between s03e and o15e and is approximately 4 km wide. There are a number of mapped lithological contacts/fractures (thin dashed lines on the map) in the MSFZ which can explain the low resistivity in F2 and F3. However, there is no indication of faults/ lithological contacts on the bedrock map between s08e and s03e (circled blue) at the location of the low resistivity area F1. The MT suggests the MSFZ to be about 6 km wide, including F1, present between s08e and s03e.

In general, the shallow subsurface mapped as mica schist displays relatively higher resistivity compared to the amphibolite units (except for s07e and s05e). However, stations between w16e and w20e in the mica schist show lower resistivity.
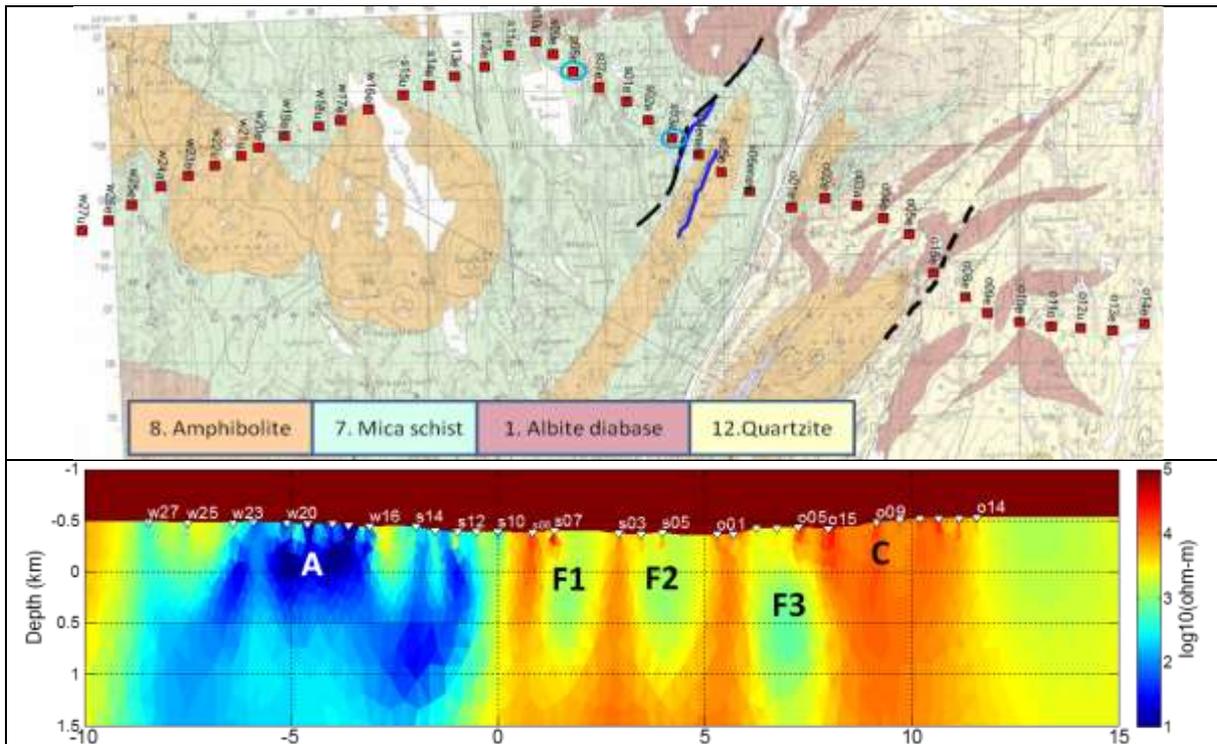
Figure 29: Geological map (top) and the MT model (bottom) along the profile. To the left of o09e, o15e, o05e, o01e and s12e there are lithological contacts characterized by lower resistivity in the MT model. Stations s17e-s19e show lower resistivity compared to other stations that are on mica schist. The quartzite to the east is associated with relatively high resistivity. Highlighted with blue and black dashed lines on the map are the locations of the Stuoragurra Fault and borders of the MSFZ respectively. The x-axis on the MT model (bottom) shows distance in km.

9.4. MT model in correlation with a DC resistivity profiles

2D resistivity profiles are from the Masi, Fiednajohka and Riednajavre areas in the Kautokeino municipality (Figure 25). The profiles show resistivity distribution in the shallow subsurface down to a maximum of about 150 m depth.

- The Masi profile maps the resistivity of mica schist and amphibolite (Figure 30). The rocks show resistivity of 2000 - 5000 Ωm with much lower values (down to about 700 Ωm) in the known fracture zones (black dashed lines). This data corroborates the observed values in the shallow western side of the MT model where these rocks dominate.
- The Fiednajohka profile crosses the Stuoragurra Fault (SF) which is also a point of interest in the MT profile. The quartzite of the Fiednajohka profile has general resistivities of 2000 - 9000 Ωm but between 1300 and 2600 Ωm across the Stuoragurra Fault (to the right of the dashed lines). These resistivities match the observations in the MT model as described in Section 9.2.
- The Riednajavre profile crosses diabase rocks and amphibolites, which in some sections host graphite. In this area the amphibolite generally reads about 1200 - 5000 Ωm but about 300 Ωm in the graphite hosted sections. Along the Masi MT profile, amphibolites are predominantly found to the west whereas albite diabase is mostly present on the eastern side. The observed resistivities in the DC resistivity profiles are consistent with the resistivities observed in the MT profile. The anomalous conductor, A, in the MT model lies in the amphibolite unit and has significantly reduced resistivity (about 30-100 Ωm).
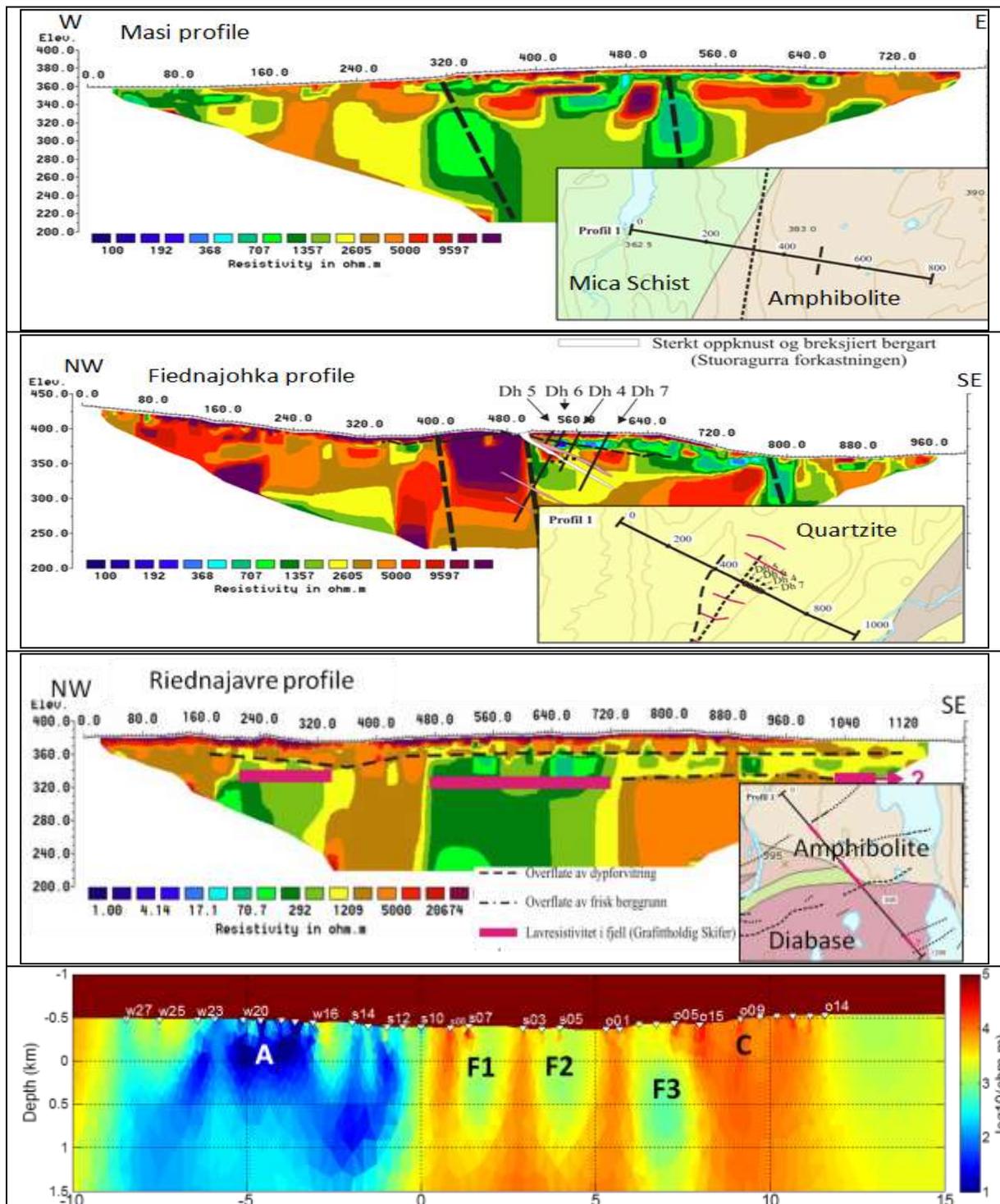
Figure 30: 2D resistivity profiles (Dalsegg & Olesen, 2014) from top: The Masi, Fiednajohka and Riednajavre profiles displayed together with the MT profile (bottom). The Y-axes of the 2D resistivity profiles are in meters, elevation above mean sea level (msl). The MT profile is in depth (km) positive downwards below msl.

9.5. Joint interpretation of the MT, seismic, magnetic and gravity data

The MT model is analysed together with seismic, magnetic and gravity data. Figure 31 shows a shallow part of model A, down to 3 km depth. Anomaly A in the MT model lies within the amphibolites of the Suoluvuobmi Formation. The top and bottom of the amphibolite unit is demarcated by resistivity boundaries which partly coincide with the seismic reflectors h1 and h3 respectively. The mica schist, which dominates the very shallow subsurface in the west and central parts of the profile, exhibits a relatively high resistivity. Anomaly C correlates with the Masi quartzite which is fractured and intruded by albite diabase. The fractured section is characterized by areas of low resistivity and some of its boundaries are marked with seismic reflectors, for example the h5 and SF reflectors (Figure 31 a). The Gål'denvarri amphibolite is found to the east of the Masi quartzite; its top is constrained by the seismic reflector h6. As observed in the resistivity log (Figure 28), amphibolites in the eastern part of the profile are characterized by relatively higher resistivity. Anomaly B is interpreted as a localised granite in the central section (Model A, Figure 32) or an extensive granite (model B, Figure 33) or an extensive gneiss (Model C, Figure 34) overlaying the higher density, low susceptibility intermediate gneiss. The interpreted models are colour coded and the definition of the colours is given in Table 2.

Model assumptions

Model A: The anomaly B is interpreted as a localised granite in the central section. This is the preferred scenario. Anomaly B, which is up to 33000 Ωm, is located in a region of a relatively high-resistivity background (about 6000 Ωm). This model separates the very high resistivity body in the central region from the background, suggesting low resistivity in the western line. This information is similar to what has been observed in the anisotropic model (Figure 38) and also from the inversion results along separate lines (Figure 23).

Model B: The anomaly B is interpreted as a granite extending towards the west. This model assumes the resistivity in the western line could be the same as that observed in the central line, and that the observed difference is due to the lack of long periods in the western area, which is why the resistivity was not well resolved.

Model C: The anomaly B is interpreted as a gneiss extending towards the west. The assumption here is similar to that of model B with the exception that the rocks are metamorphosed. The small difference in density slightly shifts the location of the base horizon. The bottom horizon is deeper on model C due to the increased density in gneiss.

Table 2: Colour codes assigned to different rocks. Density and susceptibility values are after Olesen & Solli (1985). The label 'a' refers to the mean value calculated from all samples. JGC= Jer'gul Gneiss Complex, SF= Suoluvuobmi Formation

Colour	Body name	Density (kg/m3)	Susceptibility (SI)
	SF: Mica schist	2727	0.00045
	SF: Amphibolite **a**	2950	0.00193
	Masi Formation: Quartzite **a**	2645	0.00050
	Gål'denvarri FM: Amphibolite	2950	0.00123
	Albite diabase	2918	0.24
	Albite diabase	2918	0.153
	JGC granodiorite **a**	2626	0.00095
	JGC granite **a**	2626	0.00095
	JGC gneiss	2645	0.00053
	Intermediate gneiss	2800	0.003399
	Reference	2670	0
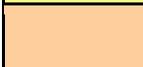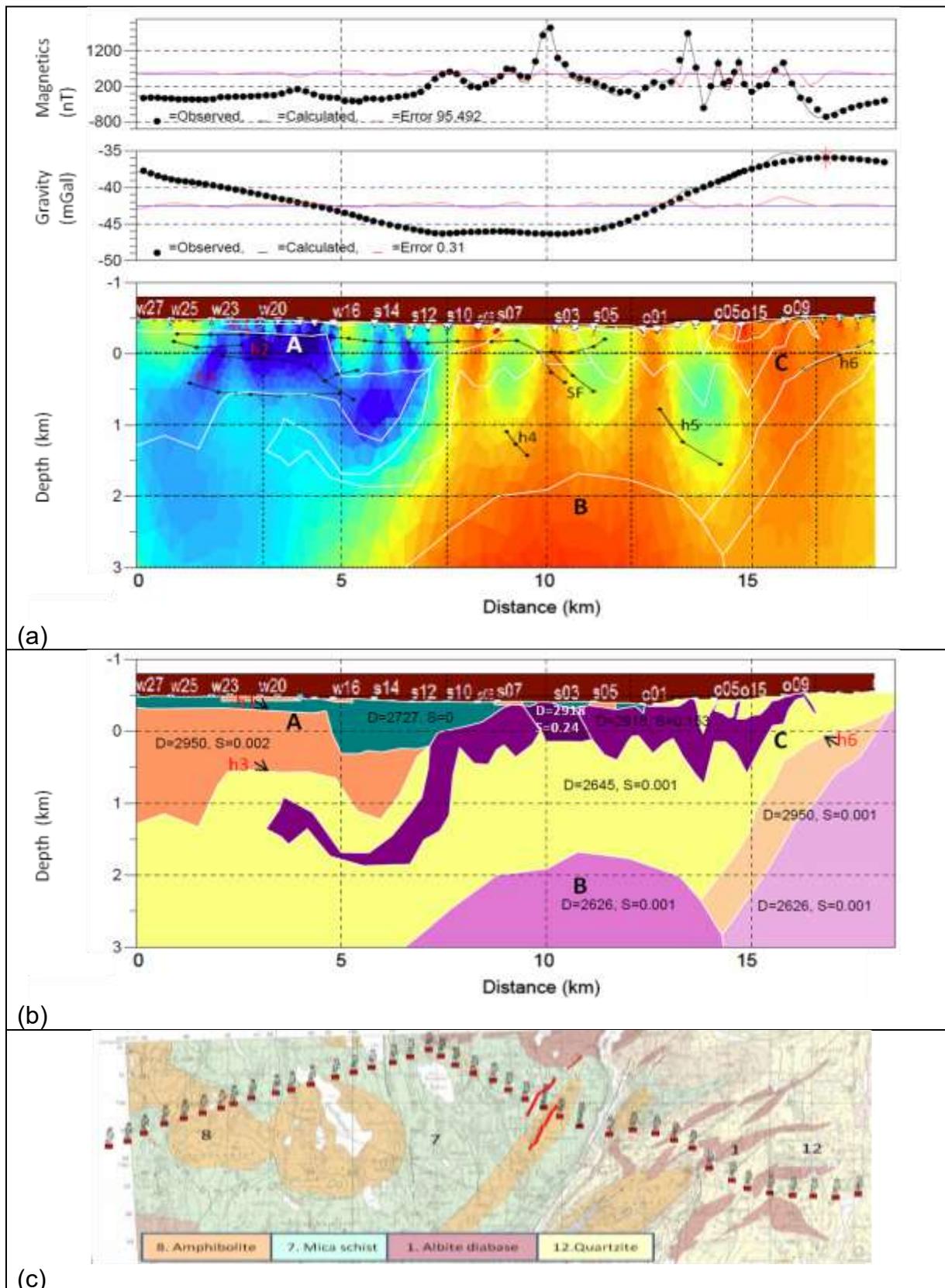
Figure 31: Magnetics and gravity data (top panels) jointly interpreted with MT resistivity model and seismic reflectors, h1-h6, SF (a). The interpreted geological model (b) is based on the MT resistivity boundaries, seismic reflectors and the geological map (c) to demarcate the density and susceptibility zones to fit the observed gravity and magnetic data respectively along the profile. The difference (red lines) between the observed data (solid circles) and the calculated (black lines) is quite small. The RMS error is 95.492 for magnetic and 0.310 for gravity data.
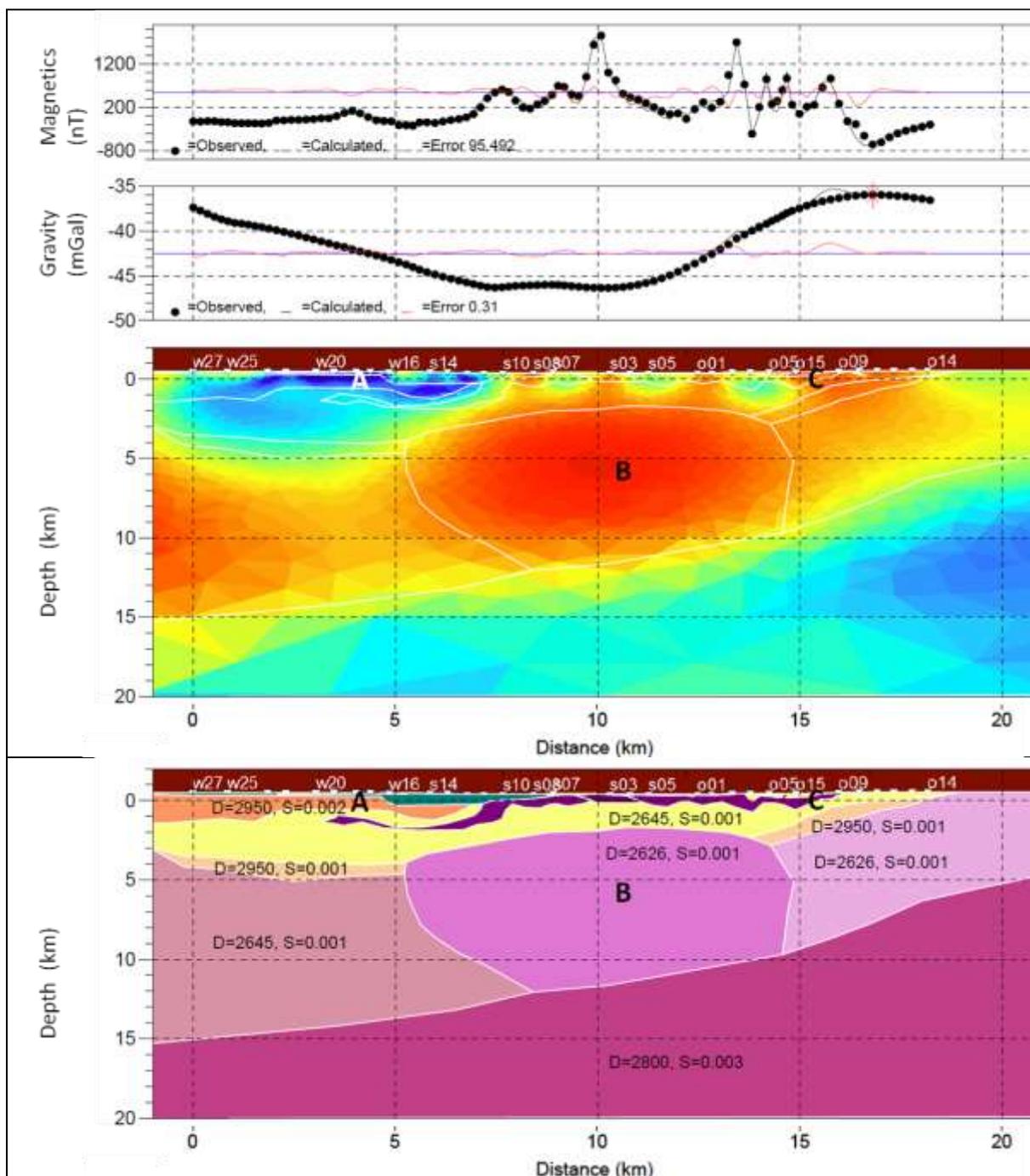
Figure 32: Model A, the anomaly B is interpreted as a localised granite in the central section and gneiss on the western side. The interpreted model (bottom) is based on the MT resistivity variations, seismic reflectors and the geological map to demarcate the density and susceptibility zones to fit the observed gravity and magnetic data respectively. The difference (red lines) between the observed data (solid circles) and the calculated (black lines) is quite small. The RMS error is 95.492 for magnetic and 0.310 for gravity data.
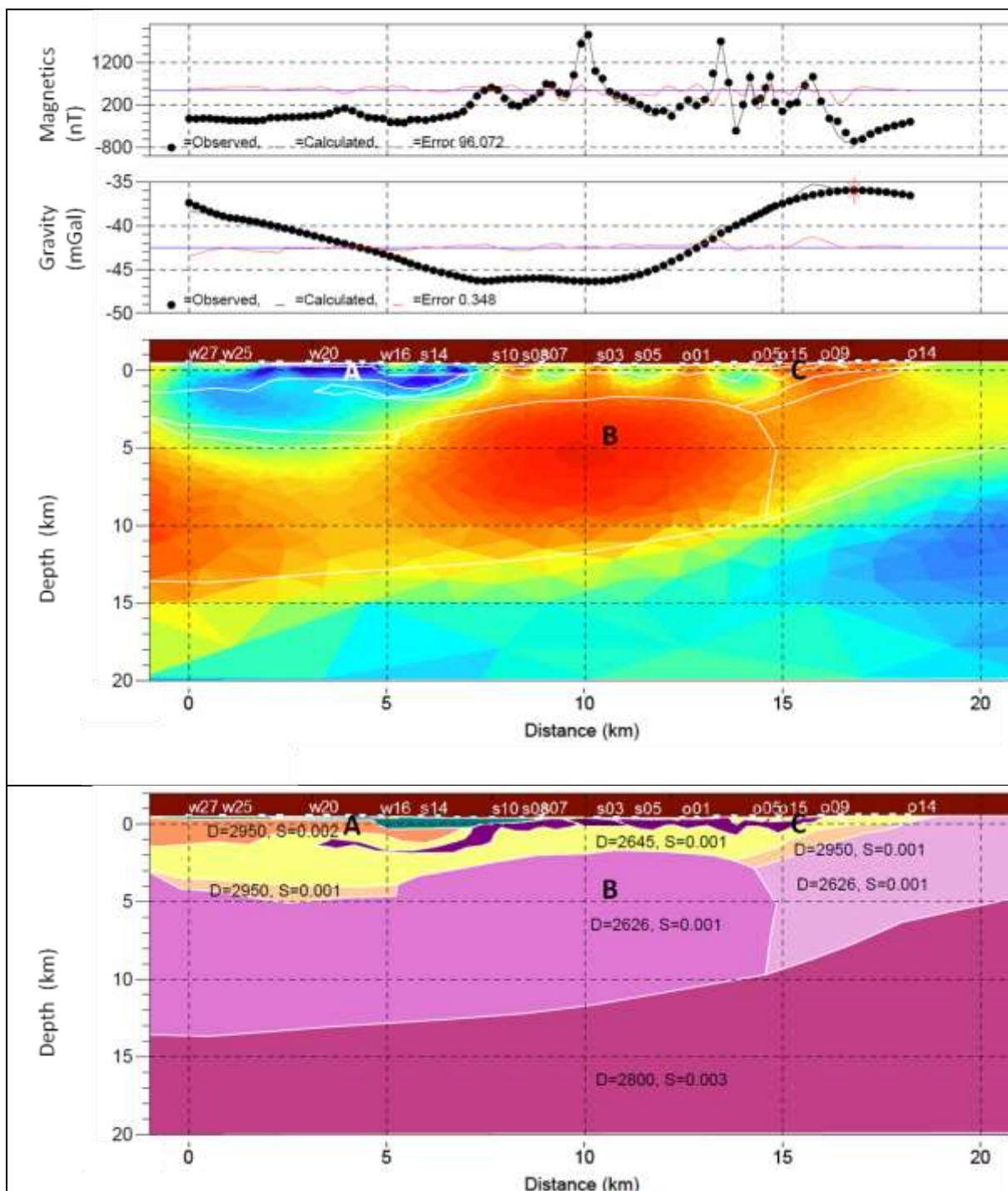
Figure 33: Model B, the anomaly B is interpreted as granite extended towards west. The interpreted model (bottom) is based on the MT resistivity variations, seismic reflectors and the geological map to demarcate the density and susceptibility zones to fit the observed gravity and magnetic data respectively. The difference (red lines) between the observed data (solid circles) and the calculated (black lines) is quite small. The RMS error is 96.072 for magnetic and 0.348 for gravity data.

Figure 34: Model C, the anomaly B is interpreted as gneiss extended towards west. The interpreted model (bottom) is based on the MT resistivity variations, seismic reflectors and the geological map to demarcate the density and susceptibility zones to fit the observed gravity and magnetic data, respectively. The difference (red lines) between the observed data (solid circles) and the calculated (black lines) is quite small. The RMS error is 96.306 for magnetic and 0.388 for gravity data.

10. DISCUSSION

It is observed from the MT inversion result that the profile is divided into four zones. From shallow to intermediate depth, there is (1) a low-resistive zone in the west down to about 5 km deep and (2) a relatively high-resistivity zone alternating with low-resistive sections in the east down to about 2.5 km deep. Below the two zones is a high-resistive layer (3) deepening towards west. At greater depth is zone (4), a low-resistive layer which is shallowing to the east.

The MT inversions carried out with different starting models produced similar results. Varying inversion parameters gave similar results regarding the main features but with differences in the thickness of the features. Therefore, the consistency of the different test results gives a reasonable confidence in the final resistivity model considering all the limitations described above. Also, the inverse modelling results correlate well with the measured data and with other resistivity measurements (DC resistivity profiles and the borehole resistivity log) available from earlier projects. Few reflectors are apparent on the seismic image but some of these are partly correlating with the resistivity boundaries.

By integrating the bedrock map, seismic section, gravity and magnetic data, the four resistivity zones are interpreted as follows:

- Zone 1 is interpreted as interbedded amphibolites, mica schists and black schists of the Suoluvuobmi Formation overlying the Masi quartzite and the Gål'denvarri amphibolite. The amphibolites are generally characterized by high density and low susceptibility. The Suoluvuobmi amphibolite is associated with very low resistivity. A conductive anomaly is found within this zone and the zone most likely hosts graphite and/or sulphides which have been reported to occur in the area (Stevenson, 1983; Dalsegg & Olesen, 2014). The schists in this zone are associated with relatively higher resistivity. The Masi quartzite is intruded by the albite diabase suggesting that it may be fractured and hence characterized by lower resistivity. Seismic data shows some reflectors in the area and together with the resistivity boundaries, lithological contacts have been established (Figure 31)

- Zone 2 is interpreted as Masi quartzite, fractured and intruded by albite diabase. It is in this zone that the postglacial Stuoragurra Fault (SF) is located. The SF location is indicated on the bedrock map as a 1 km wide fault and also seen in the seismic sections. The MT indicates the SF to be part of a 2 km wide fracture zone F2 (Figure 31) which is about 1.5 km deep. SF is hosted by the Mierujavri-Sværholt Fault Zone that is represented by the entire zone 2 section (F1 –F3). Zone 2 is interpreted as a fracture section about 6 km wide and 1.5 – 2.0 km deep. The location of the MSFZ is partly traceable in the seismic section (h5 and SF reflectors). The intruding albite diabase in zone 2 is quite shallow and some of them protrude to the surface. From the magnetic response, the albite diabase dykes/sills in the central part dip to the east while those farther to the

east dip westwards. They are mapped with relatively lower resistivity compared to the host quartzite. The diabase dykes are characterized by significantly higher magnetic susceptibility and density. Their presence is vital in the modelling of the observed magnetic field. However, they are too thin to dominate the regional gravity field. The gravity data in the central part is dominated by the quartzite. Its lower density leads to a pronounced gravity low. Beyond the Masi Quartzite to the east is the high-density Gål'denvarri amphibolite and a granodiorite, all of which are low in susceptibility. As recorded in the Vuottasjavri resistivity log (Figure 28), the resistivity of the amphibolite (Gål'denvarri) is not dinstict from the neighbouring rocks and was therefore not resolved (distinguished) in the MT data. However, it is characterized by relatively higher density, 2900 kg/m^3 (and probably higher P-wave velocity) compared to the surrounding quartzite (2645 kg/m^3) and granodiorite (2660 kg/m^3). This leads to a strong acoustic impedance contrast and therefore the top horizon of the Gål'denvarri was reflected in the seismic data (labelled h6 in Figure 31). h6 is probably not a single reflector. h6 is more likely composed of several shorter reflectors related to the complex patterns of amphibolites and diabase dykes in the area.

- Zone 3 is interpreted as granite and/or gneiss. They are both low in susceptibility. The gneiss has a density of 2645 kg/m^3 and the granite has a density of 2626 kg/m^3. Their difference in density slightly affects the interpreted position of their bottom horizon. The bottom horizon is shallower in the granite model than in the gneiss model. This allows for the high-density underlying layer to come shallower to compensate for the reduced density in the granite layer.

- Zone 4 is interpreted as an intermediate gneiss with a density of 2800 kg/m^3. The interpreted shallowing of zone 3 and 4 towards the east reflects the observed higher values of the gravity fields in the area.

Generally, there is a good correlation between the different data sets. The combined differences in resolution and/or sensitivity to the various rock properties is an advantage for a comprehensive understanding of the subsurface.

11. CONCLUSION

The geology of the Masi region has been extensively studied and there is a considerable amount of geological, petrophysical and geophysical information of the area. However, most of this information provides only knowledge of the shallow subsurface. Magnetotelluric data at Masi was collected in 2015. The main objective is to understand the regional and deep geology in the area and especially the settings of the postglacial Stuoragurra Fault. Having a range of high to low frequencies, MT data has a great depth of penetration and is a useful tool in the understanding of the deep subsurface.

To mitigate the interpretation ambiguity caused by the none-uniqueness of the forward and inverse modelling, MT was jointly interpreted with seismic, bedrock, gravity and magnetic data. The MT model was verified by its consistency in the range of resistivities as observed on the DC resistivity profiles and the resistivity log on identified lithologies.

The MT resistivity model categorizes the surveyed region into four distinct zones. To the west down to about 5 km depth is a low-resistivity zone interpreted as the Suoluvuobmi Formation comprised of interbedded amphibolites, mica schists and black schists overlying the Masi Formation. To the east, down to about 2.5 km depth, is a relatively high-resistive zone alternating with low resistivity sections. Zone 2 is interpreted as Masi quartzite fractured and intruded by albite diabase dykes. Zone 3 is a relatively high-resistive layer below zones 1 and 2 and is interpreted as granite and/or gneiss. Zone 4 is a relatively low-resistive layer underlying zone 3; it is interpreted as intermediate gneiss.

The postglacial Stuoragurra Fault (SF) is located within the Mierujavri-Sværholt Fault Zone (MSFZ) that is represented by a fractured section of zone 2. The fractured section is about 6 km wide and 1.5 – 2.0 km deep. The SF is about 2 km wide and 1.5 km deep. The locations of the SF and MSFZ are partly evident on the seismic section and are also indicated on the geological maps.

MT lacks resolution to resolve thin horizontal layers and small resistivity contrasts between adjacent layers. The availability of seismic and other geological and geophysical data is of great advantage in the interpretation of the observed resistivity zones.

The low-resistive zone in the shallow western side of the profile might indicate a potential for mineral resources. However, a complete understanding of the lithology will only be achieved by drilling.

12. REFERENCE

Becken, M. and Burkhardt, H., 2004: An ellipticity criterion in magnetotelluric tensor analysis. *Geophys. Journal Int. 159, 69–82*, https://doi.org/10.1111/j.1365-246X.2004.02376.x.

Bingen, B., Solli, A., Viola, G., Torgersen, E., Sandstad, J.S., Whitehouse, M.J., Røhr, T.S., Ganerød, M. & Nasuti, A., 2016: Geochronology of the Palaeoproterozoic Kautokeino Greenstone Belt, Finnmark, Norway: Tectonic implications in a Fennoscandia context. *Norwegian Journal of Geology 95*, 365–396, http://dx.doi.org/10.17850/njg95-3-09.

Cagniard, L., 1953: Basic theory of the magnetotelluric method of geophysical prospecting. *Geophysics 18*, 605–635.

Caldwell, T. G., Bibby H. M., and Brown, C., 2004: The magnetotelluric phase tensor *Geophys. Journal. Int. 158*, 457–469.

Chave A.D & Jones, A. G., 2012: The Magnetotelluric method: Theory and practice. *Cambridge university press, New York*, 552 pp.

Constable, S.C., Parker, R.L. & Constable, C.G., 1987: Occam's inversion - a practical algorithm for generating smooth models from electromagnetic sounding data. *Geophysics*, 52 (03), 289–300.

Egbert, G.D & Booker, J.R., 1986: Robust estimation of geomagnetic transfer functions. *Geophys. Journal of the Royal Astronomical Society, 87, 173-194.*

Eiken, O., Degutsch, M., Riste, P. and Rød, K., 1989: Snowstreamer: an efficient tool in seismic acquisition. First Break, 7(9), 374-378.

Elvebakk, H., 2011: Geofysisk logging av borehull ved Vuottasjavri og Bidjovagge, Kautokeino, Finnmark. *NGU rapport nr. 2011.010*, 36 pp.

Johansen, T.A., Ruud, B.O., Bakke, N.E., Riste, P., Johannessen, E., & Henningsen, T., 2011: Seismic profiling on Arctic glaciers. First Break, 29(2), 29-35.

Key, K., 2012: Marine EM inversion using unstructured grids: a 2D parallel adaptive finite element algorithm. *SEG Technical Program Expanded Abstracts* 1–5, https://doi.org/10.1190/segam2012-1294.1

Key, K., 2016: MARE2DEM: a 2-D inversion code for controlled-source electromagnetic and magnetotelluric data. *Geophysical Journal International* 207, 571–588, https://doi.org/10.1093/gji/ggw290.

Naidu, G. D., 2012: Deep Crustal Structure of the Son–Narmada–Tapti Lineament, Central India. *Springer Theses* 13-35, DOI: 10.1007/978-3-642-28442-7_2.

Olesen, O. and Dalsegg, E., 2014: Resistivitetsmålinger ved Masi, Fiednajohka og Riednajavre og implikasjoner for malmleting, Kautokeino kommune, Finnmark. *NGU Rapport 2014.021, 28* pp.

Olesen, O. and Sandstad, J. S., 1993: Interpretation of the Proterozoic Kautokeino Greenstone Belt, Finnmark, Norway from combined geophysical and geological data. *NGU Bulletin 425*, 43-62

Popowski, T., Connard, G., and French R., 2009: GM-SYS Profile Modeling: gravity and magnetic Modeling Software for Oasis montaj™. USER GUIDE V 4.1

Schmidt, L. M., 2016: Source effects in magnetotelluric array: Data from northern Norway. *Master thesis, University of Munster*, 65 pp.

Siripunvaraporn, W., Egbert, G and Uyeshima, M., 2005: Interpretation of two-dimensional magnetotelluric profile data with three-dimensional inversion: synthetic examples. *Geophys. Journal Int. 160*, 804–814

Solli, A. 1988: Masi, /933 IV, berggrunnsgeo/ogisk kart M l: 50 000. Norges geologiske undersøkelse, Trondheim.

Stevenson, D.B., 1983: Masi project: N-82-4, *Annual report*, 168 pp.

Stevenson, D.B., 1984: Masi project: N-81-4, *Annual report*, 83 pp.

Thiel, S. 2008: Modelling and inversion of magnetotelluric data for 2-D and 3-D lithospheric structure, with application to obducted and subducted terranes. *Ph.D Thesis University of Adelaide, School of Earth and Environmental Sciences*, 154 pp.

Unsworth, M. J., 2007: Magnetotellurics. In: Gubbins, D., Herrero-Bervera, E. (Eds.) Encyclopedia of geomagnetism and paleomagnetism. *Springer, Dordrecht, 207,* 670-673. https://doi.org/10.1007/978-1-4020-4423-6_207.

Vozoff, K., 1991: The magnetotelluric method: Electromagnetic methods in applied geophysics. *Society of Exploration Geophysicists*, 2B, 641−711.

A. APPENDIX

A.1.   Testing starting models

The half space starting model had an initial misfit of RMS error 21.2 and converged to RMS error 2.03 at iteration 13. A structured starting model, named Model5v2 had an initial misfit of RMS error 12.93 and converged to RMS error 2.44 at iteration 12. All starting models converged to similar final models. The test is run using a spatial horizontal/vertical weight (w_{hv}) of 1, a Lagrange multiplier (μ) of 2 and isotropic. The results imply the inversion code to be robust and less influenced by initial models.
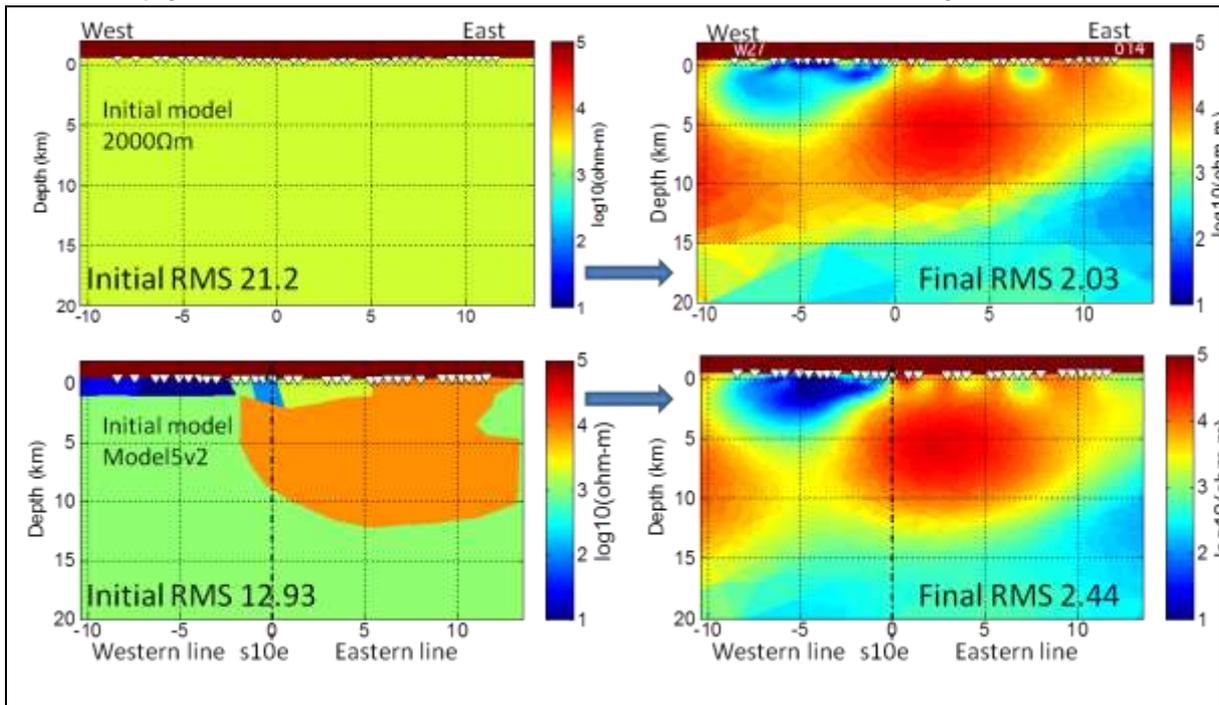

Figure 35: Starting models to the left and inverse models to the right. Regardless of the starting models, the final models are similar. Station s10e at 0 km on the x-axis is at the junction of the western and eastern lines. White triangles at the top show the MT stations.

A.2. Testing spatial vertical/horizontal weight

The spatial horizontal to vertical penalty weight, w_{hv} is a smoothness regularization parameter (see section 5). $w_{hv} > 1$ biases the inversion towards enhanced horizontal smoothness, while for $w_{hv} < 1$, vertical smoothness is enhanced. To find w_{hv} for best results, the test is run using a Lagrange multiplier (μ) of 2 and an isotropic, structured starting model named Model5v2. For $w_{hv} = 0.5$ and $w_{hv} = 3.0$, the inversion converged to RMS error of 2.5. For $w_{hv} = 1.0$, the inversion converged to RMS error of 2.4. Based on the misfit and visual assessment, $w_{hv} = 1.0$ seems to give the best results.
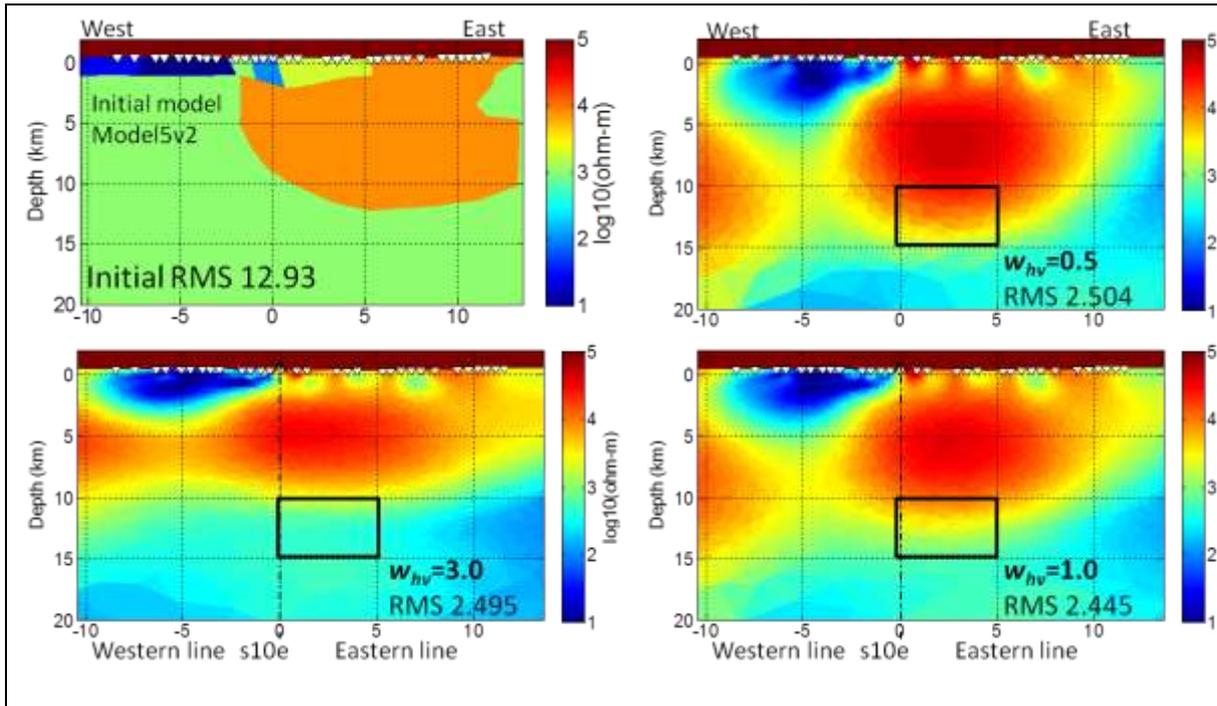

Figure 36: whv test: Top left profile shows the starting model. Final model, whv =0.5 (top right) shows anomalies extending to larger depths. Note that both the anomalous conductor and resistors seem to be dragged down. As observed in the black box area, the resistor is deeper with whv =0.5 and gets thinner as whv increases. Looking at the RMS misfit, whv =1 seems to give the best fit.

A.3. Testing anisotropy penalty weight

Figure 37 and Figure 38 show isotropic and anisotropic (transverse isotropic z direction, TIZ) inversions, respectively. Parameter settings are shown in Table 3.

Table 3: A summary of parameter settings for anisotropic tests.

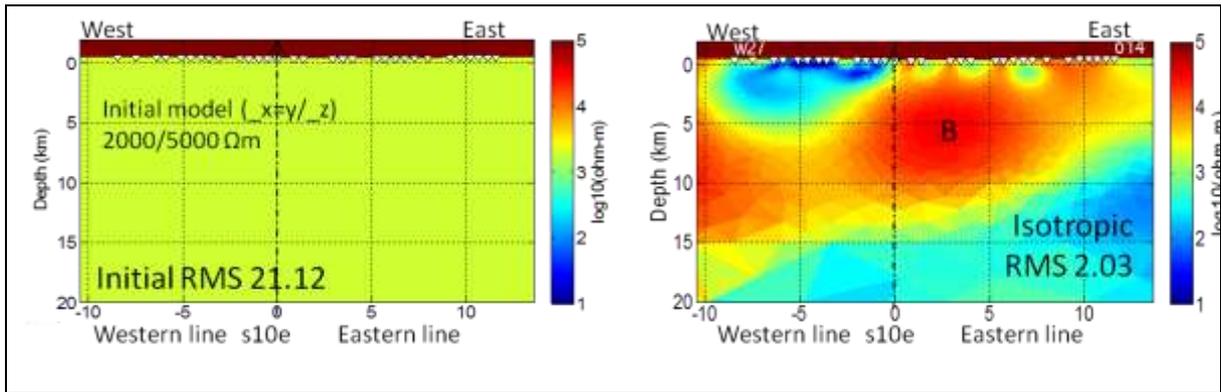| TM mode inversion	Half space start model (Ωm)	W_{hv}	μ	α	Initial Misfit	Final Misfit RMS@iteration	Comments on final models
Isotropic	2000	1	2	-	21.2	2.03@13	Isotropic model
TIZ_0p1	2000/2000	1	2	0.1	21.2	2.41@11	Anisotropic models
TIZ_1p0	2000/2000	1	2	1.0	21.2	2.32@11	Isotropic models

Figure 37: An isotropic inversion test. To the left is a half-space starting model. To the right is a resulting isotropic inverse model. The inversion had an initial misfit of RMS error 21.2 and converged to RMS error 2.03 at iteration 13.
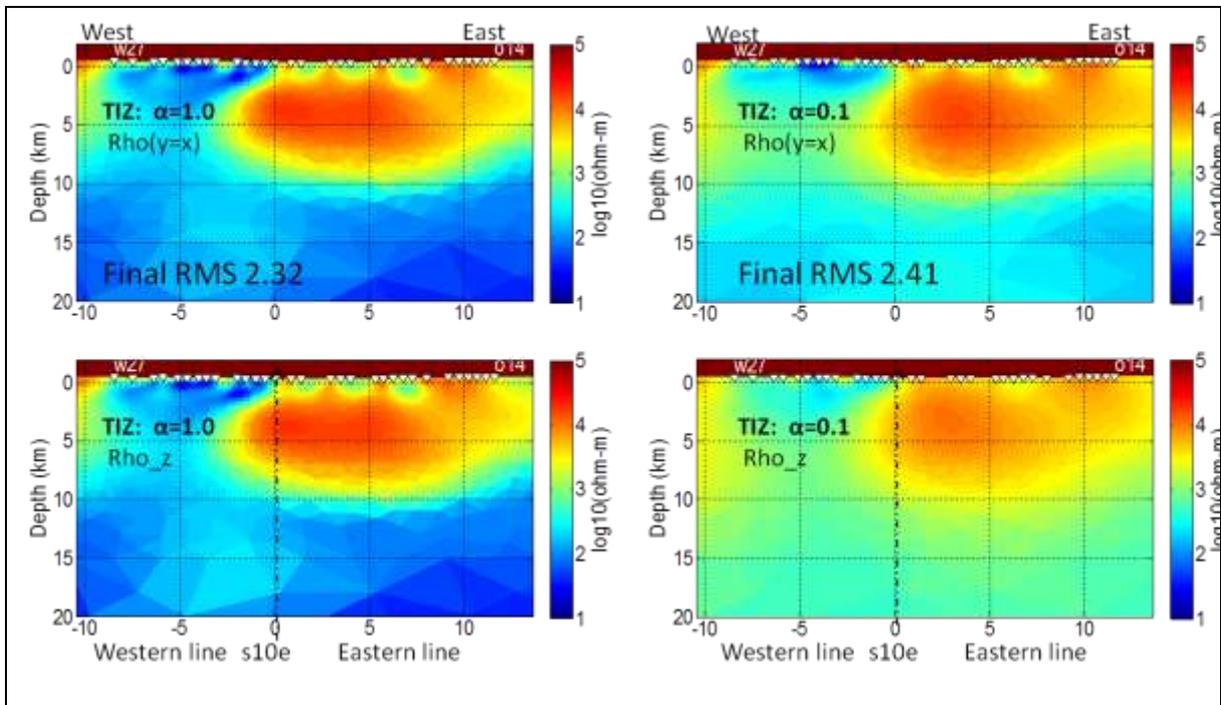

Figure 38: TIZ anisotropic inversion: α =1.0 (left) and α =0.1 (right). Top images are Rho_y=Rho_x models and bottom images are Rho_z models. α =1.0 gives isotropic models, Rho_y=Rho_x= Rho_z while α =0.1 gives anisotropic models, Rho_y=Rho_x≠ Rho_z.

The isotropic model is preferred due to a low misfit but also based on the assumption of interpreting the high resistive body (anomaly B) as continuously extending towards the west. The differences in the deep section on the western side could be due to lack of long periods at this side and hence a low sensitivity to the variations in the model or due to decoupling of the y and z components in the anisotropic case.

GEOLOGICAL
SURVEY OF
NORWAY
· NGU ·